Observation of Porosity Reduction in a Densification-Prone Test Fuel Rod: Data and Analysis

Prepared by M. E. Cunningham, J. L. Daniel, D. D. Lanning

Pacific Northwest Laboratory
Operated by
Battelle Memorial Institute

Observation of Porosity Reduction in a Densification-Prone Test Fuel Rod: Data and Analysis

Prepared by
M.E. Cunningham, J.L. Daniel, D.D. Lanning

Pacific Northwest Laboratory
Richland, WA 99352

ACKNOWLEDGMENTS

ABSTRACT

Instrumented fuel assembly (IFA)-431 was irradiated in the Halden Boiling Water Reactor (HBWR) for the purpose of extending the steady-state data base. Rod 6 of this assembly began irradiation with UO_2 fuel of 92% theoretical density (TD) that was unstable with respect to in-reactor densification. Thermal resintering tests resulted in a final density of 95.3% TD while post-irradiation examination (PIE) indicated a final density of 96.5% TD. Observed microstructural changes were consistent with published densification studies; there was a marked depletion of submicrometer diameter pores and total pore volume. However, grain size increased only slightly, indicating that internal pellet temperatures did not reach the 1875K applied in resintering tests.

Densification was observed to increase the temperatures in rod 6, but temperatures did not become as high as for a sibling rod that simulated instantaneous densification.

Temperatures calculated with U.S. Nuclear Regulatory Commission (NRC) fuel performance computer codes were generally higher than observed temperatures.

SUMMARY

In-reactor densification of UO_2 fuel can have significant effects on the thermal and mechanical performance of nuclear fuel rods. To provide additional data on the irradiation behavior of densifying fuel, rod 6 of instrumented fuel assembly (IFA)-431 contained fuel of 92% theoretical density (TD) that was unstable with respect to in-reactor densification. Following an extensive pre-irradiation characterization, IFA-431 was irradiated from June 1975 to February 1976 and then subjected to postirradiation examination (PIE) during 1977 and 1978.

Thermal resintering tests during the precharacterization showed a density change from 92 to 95.3% TD, and PIE measurements indicated a final density of 96.5% TD after a rod average burnup of approximately 380 GJ/kgU (4400 MWd/MTM).

Observed microstructural changes after irradiation were consistent with the measured in-reactor densification, including a marked depletion of submicrometer pores and an accompanying reduction in total pore volume proportional to pellet burnup. Grain size increased only slightly with irradiation (from an average of 6 µm preirradiated to 8 µm irradiated) although resintering tests at 1875K on sibling pellets produced grains averaging 16 µm. Pronounced accumulation of porosity at the grain boundary occurred near the axis of the higher burnup pellets.

Fuel centerline temperature measurements from rod 6 have been compared to those from rod 1 (standard BWR-6) and rod 2 (large initial fuel-cladding gap to simulate instantaneous isotropic densification). Temperatures during the first power ascension showed that rod 6 had higher temperatures than rod 1 but lower temperatures than rod 2. Rod 6 temperatures did increase as a result of densification but never became as high as those in rod 2. It was therefore concluded that the temperature effect of densification is not as severe as instantaneous isotropic densification.

Temperature data from IFA-431 has also been compared to calculations performed by the U.S. Nuclear Regulatory Commission (NRC) fuel performance computer codes. In general, temperatures calculated by the codes, when using a

densification model, were higher than observed temperatures. An uncertainty band for the calculated temperatures overlapped the observed temperatures in a number of cases.

CONTENTS

FIGURES

TABLES

INTRODUCTION

If a loss-of-coolant accident (LOCA) should occur in a light water reactor (LWR), the short-term thermal stored energy and the long-term fission product decay heat of the fuel become the driving forces for fuel rod damage. To assess both the amount of energy that is present and its rate of removal, the U.S. Nuclear Regulatory Commission (NRC) relies on fuel performance computer codes that are designed to account for both fuel rod design and operating conditions. However, the individual models within a code and the net result of their interactions are continually being evaluated for accuracy and validity.

In 1972 it was discovered that the fuel in some commercial fuel rods had undergone considerable densification that resulted in a decreased fuel volume, increased radial and axial gaps, and some cladding deformation due to coolant pressure. The immediate concern was the effect that densification could have upon fuel rod behavior during LOCA conditions. The NRC quickly set forth requirements that placed restrictive limits on reactor operation.[1] Fuel vendors in turn examined their data and developed models to describe the densification behavior of UO_2.[2,3,4] In addition, programs were initiated to better understand densification and to determine the characteristics of densification-resistant fuel.[5-9]

By 1974, the NRC had approved vendor models that calculated densification as a function of time or burnup.[10] Fuel that was made up of large UO_2 grains and a small fraction of small pores (<1 μm) was found to be densification resistant. Calculations of fuel rod thermal behavior, now accounting for densification, were considered to be improved over pre-1972 calculations. However, in-reactor data for comparison to the code calculations was still sparse.

In 1974 the NRC began sponsoring the Experimental Support and Development of Single-Rod Fuel Codes Program at Pacific Northwest Laboratory (PNL)[a] to provide a data base for the development and verification of NRC audit and best-estimate codes. Recognizing the need for in-reactor thermal data on densifying

---

(a) Operated for the U.S. Department of Energy (DOE) by Battelle Memorial Institute.

1

fuel, one objective of the program was to include densifying fuel in the design of test irradiation rigs. The overall design of those instrumented fuel assemblies (IFAs)--IFA-431 and IFA-432--was predicated on the need to obtain as much information as possible. Thus, each of the six rods in each assembly[a] was of a different but interrelated design, which allows cross comparison of the irradiation behavior due to design differences. Rod 6 is of specific interest since it contained pellets that were not resistant to in-reactor densification.

IFA-431 was irradiated from June 1975 to February 1976 in the Halden Boiling Water Reactor (HBWR), Halden, Norway, and then removed; IFA-432 began irradiation in December 1975 and completed irradiation in June 1981. During 1977 and 1978, destructive postirradiation examination (PIE) was performed on rod 6 of IFA-431 by AERE[b] Harwell, U.K.; and a final report on their findings was issued to PNL late in 1978. The PIE included bulk and microdensity changes and metallographic examination of porosity changes. A general report discussing the irradiation of IFA-431 has been released.[11] Because PIE data has been obtained only for rod 6 of IFA-431, this report will concentrate on that rod. Some supporting in-reactor data for rod 6 of IFA-432 will also be presented.

In recent years vendors have changed to densification-resistant fuels, thus reducing the need for further extensive evaluation of densifying fuel. Recognizing this change in emphasis, this report will present the observed thermal behavior of rod 6, an analysis of fuel microstructural changes due to irradiation, and a comparison of current fuel performance computer codes to the thermal data. However, this report will not present an analysis of densification kinetics.

(a) IFA-431 and IFA-432 are identically designed assemblies.
(b) Atomic Energy Research Establishment.

2

EXPERIMENTAL DESIGN

In addition to studying the effects of fuel density and stability, the test parameters for IFA-431 and IFA-432 include three fuel-cladding gap sizes, two fill gas compositions, and different operating power levels. To monitor the performance of the fuel rods, each rod in each assembly was instrumented with two fuel centerline thermocouples and a cladding axial elongation sensor. Three of the rods in each assembly were also equipped with fill gas pressure transducers. Self-powered neutron detectors (SPNDs) determine local linear heat rates in each assembly. The precharacterization report for the two assemblies[12] contains a full description of the assemblies and a discussion of the objectives. Table 1 provides a summary of design characteristics, and Figure 1 is a schematic of the assemblies.

Rods 1, 2, and 6 are of particular concern in this analysis. The basic design features of these rods are:

- Rod 1 serves as the standard or reference rod for this program. It simulates a typical BWR-6 fuel rod and was fabricated with stable fuel of 95% theoretical density (TD), a fuel-cladding gap of 230 µm, and helium fill gas. The active fuel length was 0.57 m for all rods.

- Rod 2 simulates a fuel rod with unstable fuel of 92% TD that instantaneously densified to 96.5% TD. The fabricated rod had a fuel-cladding gap of 380 µm, 95% TD stable fuel, and helium fill gas.

- Rod 6 is a fuel rod with densifying fuel that was initially 92% TD but was unstable with respect to in-reactor densification. The initial fuel-cladding gap was 230 µm, and the fill gas was helium.

TABLE 1. Design Parameters and Instrumentation for IFA-431 and IFA-432

IFA-431 Peak Power - 33 kW/m

Rod No.	Pellet Diameter, mm	Cold Diametral Gap,(a) μm	Fill Gas	Fuel Density, % TD	Fuel Type(b)	Instrumentation			
						Temperature			Cladding
						Upper	Lower	Pressure	Length
1	10.681	230	He	95	Stable	TC(c)	TC	PT(d)	ES(e)
2	10.528	380	He	95	Stable	TC	TC	--	ES
3	10.858	50	He	95	Stable	TC	TC	--	ES
4	10.681	230	Xe	95	Stable	TC	TC	--	ES
5	10.681	230	He	92	Stable	TC	TC	PT	ES
6	10.681	230	He	92	Unstable	TC	TC	PT	ES

IFA-432 Peak Power - 49 kW/m

Rod No.	Pellet Diameter, mm	Cold Diametral Gap,(a) μm	Fill Gas	Fuel Density, % TD	Fuel Type(b)	Temperature Upper	Temperature Lower	Pressure	Cladding Length
1	10.681	230	He	95	Stable	TC	TC	PT	ES
2	10.528	380	He	95	Stable	UT(f)	TC	--	ES
3	10.833	70	He	95	Stable	TC	TC	--	ES
4	10.681	230	Xe	95	Stable	TC	TC	--	ES
5	10.681	230	He	92	Stable	TC	TC	PT	ES
6	10.681	230	He	92	Unstable	TC	TC	PT	ES
7	10.528	380	He	95	Stable	--	--	--	--
8	10.681	230	He	95	Stable	--	--	--	--
9	10.732	180	He	95	Stable	--	--	--	--

(a) Cladding for all rods had an outside diameter (OD) of 12.789 mm and an inside diameter (ID) of 10.909 mm; diametral gap = cladding ID minus pellet diameter.
(b) With respect to in-reactor densification.
(c) TC = thermocouple.
(d) PT = pressure transducer.
(e) ES = elongation sensor.
(f) UT = ultrasonic thermometer.

4

SEAL GLAND

FAILURE MONITOR
STEAM SAMPLER

▽ 2400 mm WATER LEVEL
— 2278 mm

OUTLET THERMOCOUPLES

OUTLET TURBINE VELOCITY METER

GUIDE TUBE
ALUMINUM FLOW TUBE

A   A

3 PRESSURE TRANSDUCERS
6 FUEL RODS
6 FUEL CENTER THERMOCOUPLES
3 VANADIUM NEUTRON DETECTORS
1 COBALT NEUTRON DETECTOR
3 VANADIUM NEUTRON DETECTORS
6 FUEL CENTER THERMOCOUPLES
6 CLADDING ELONGATION SENSORS
INLET THERMOCOUPLES
INLET TURBINE VELOCITY METER
CALIBRATION VALVE
CORE BASE PLATE

▼ 1102 mm
▼ 1008 mm
▼ 804 mm
▼ 586 mm
▼ 517 mm
▼ 285 mm

NATURAL CIRCULATION
NORMAL OPERATION

0 mm

FORCED CIRCULATION, CALIBRATION ONLY

A-A
ND4
6 1
5 2
ND6 ND5
4 3

B-B
ND1
6 1
5 2
ND3 ND2
4 3

FIGURE 1. Schematic of IFA-431

5

The assemblies have been irradiated in the HBWR, which uses natural circulation of heavy water for cooling and has the following operating parameters:

Power Level	12 MWth
Reactor Coolant Pressure	3.45 MPa
Heavy Water Saturation Temperature	513K
Coolant Inlet Temperature	510K
Thermal Neutron Flux	2×10^{16} n/m^2-s per W/gUO$_2$
Fast Neutron Flux (>1 MeV)	5×10^{15} n/m^2-s per W/gUO$_2$
Average Power Density	14.8 W/gUO$_2$

Data is recorded every 15 min by a computer-controlled acquisition system and is then sent to PNL for appropriate corrections (e.g., axial flux shape and radial flux tilt) and analysis.
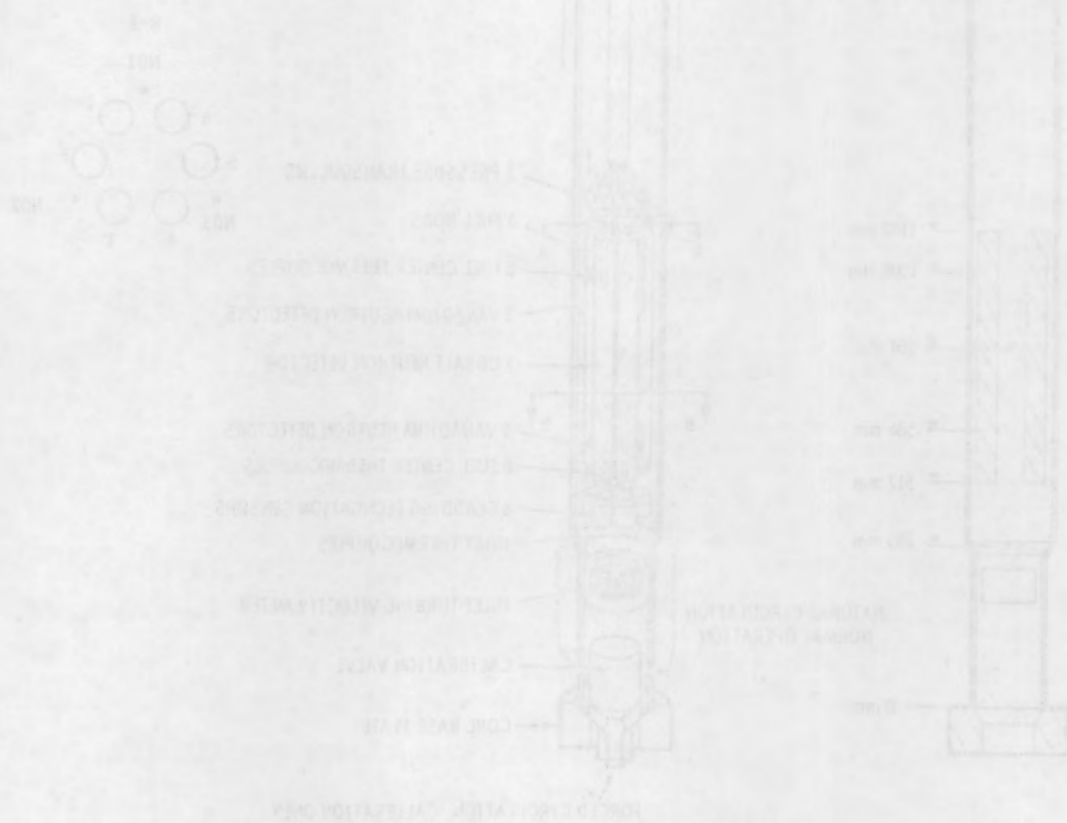
IRRADIATION HISTORY AND THERMAL ANALYSIS

The irradiation of IFA-431 began June 8, 1975, and ended February 13, 1976. When the assembly was removed from the reactor, the average burnup was approximately 380 GJ/kgU (4400 MWd/MTM); Table 2 lists the local end-of-life (EOL) burnups for the six rods in IFA-431. After cooling for 123 days, IFA-431 was shipped to the Kjeller Hot Lab, Kjeller, Norway, for nondestructive examination (NDE) of all rods. Rod 6 was then sent to AERE Harwell, U.K., for destructive PIE to determine fission gas release, microstructural changes, density changes, and burnup analysis; this work was completed in August 1978.

TABLE 2. End-of-Life Burnup for IFA-431

Thermocouple Position	Local Burnup, GJ/kgU[a]					
	Rod 1	Rod 2	Rod 3	Rod 4	Rod 5	Rod 6
Lower	314	324	336	325	315	308
Upper	432	447	463	449	434	425
Rod Average	373	386	400	387	375	367

(a) MWd/MTM = GJ/kgU x 11.574.

The irradiation history of IFA-431 is summarized in Figure 2 where reactor power and assembly average burnup are plotted as a function of real time. Linear heat rates at the upper and lower thermocouples of rod 6 are presented in Figures 3 and 4 as a function of local burnup, and corresponding centerline temperatures are shown in Figures 5 and 6.

Thermal resistance has been found to be a useful aid in the analysis of fuel rod thermal behavior. As the heat transfer behavior of a fuel rod changes (e.g., due to densification, fuel cracking, and/or fission gas release), the thermal resistance changes. Specifically, thermal resistance is the ratio of the difference between the fuel centerline temperature and the coolant temperature to the local linear heat rate:

$$R_T = \frac{T_{CL} - T_W}{LHR \times 1000}$$

7
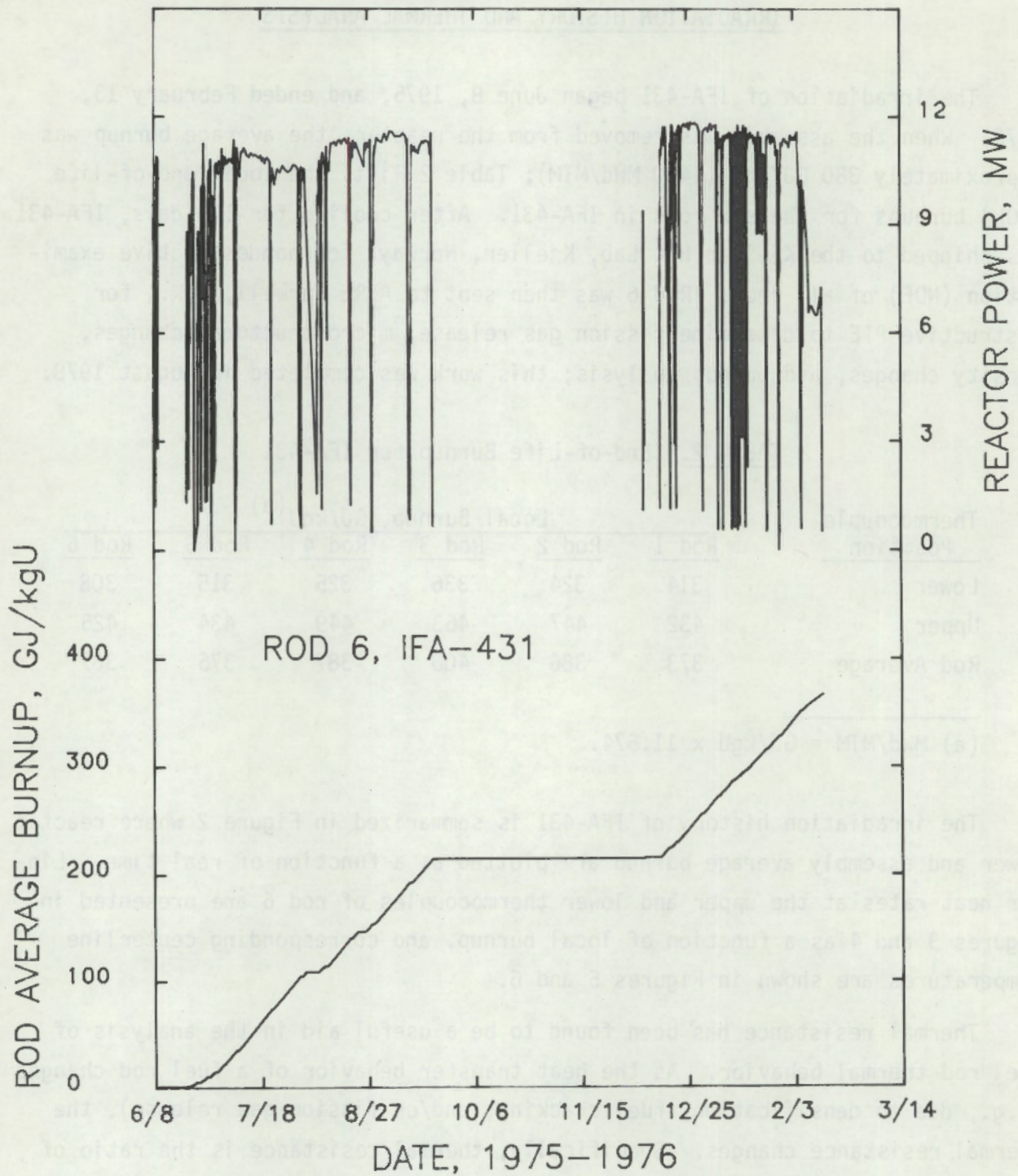
FIGURE 2. Overview of Irradiation Power History for IFA-431 with Rod Average Burnup for Rod 6

8
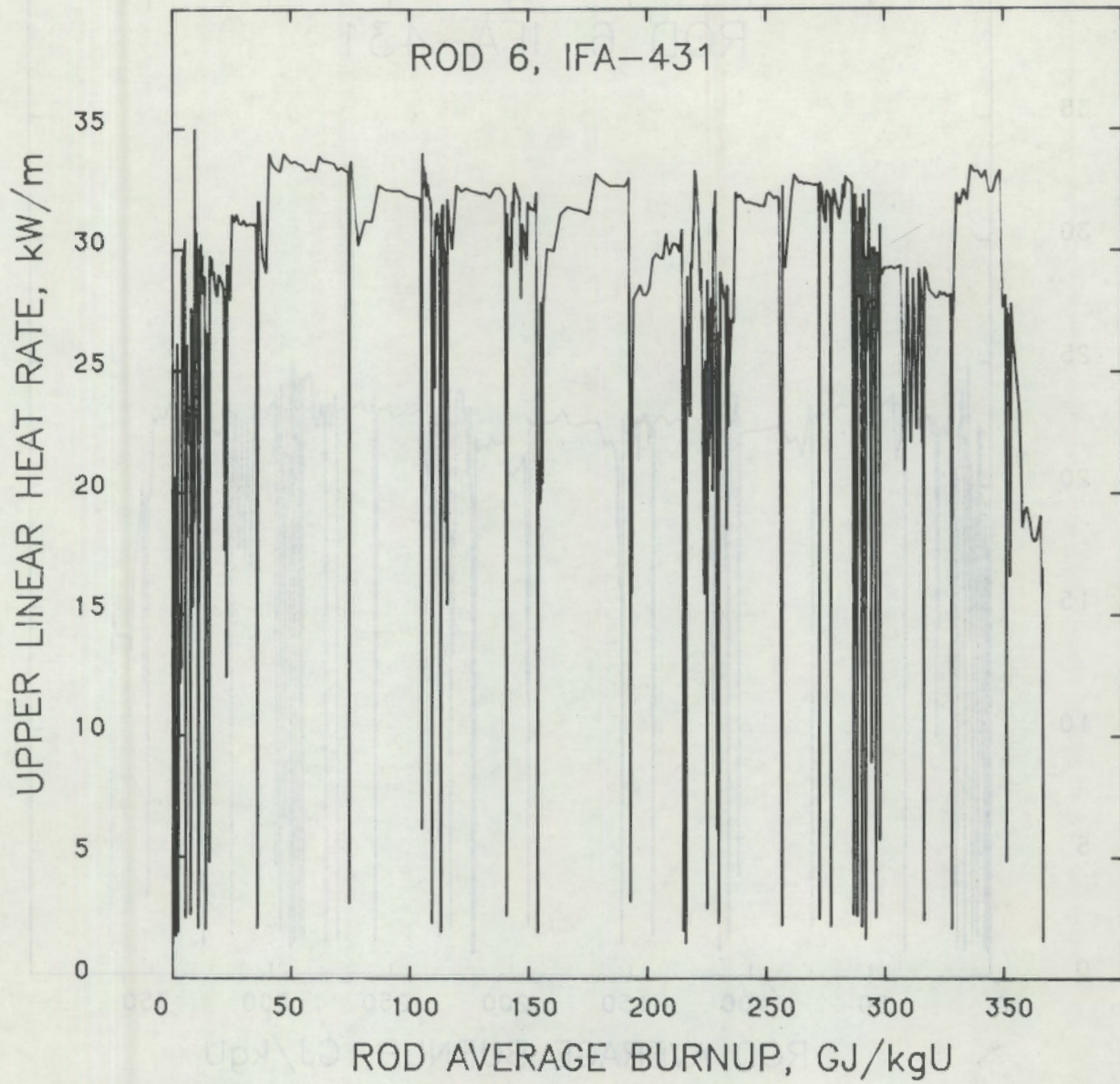
FIGURE 3. Upper Linear Heat Rate for Rod 6 of IFA-431
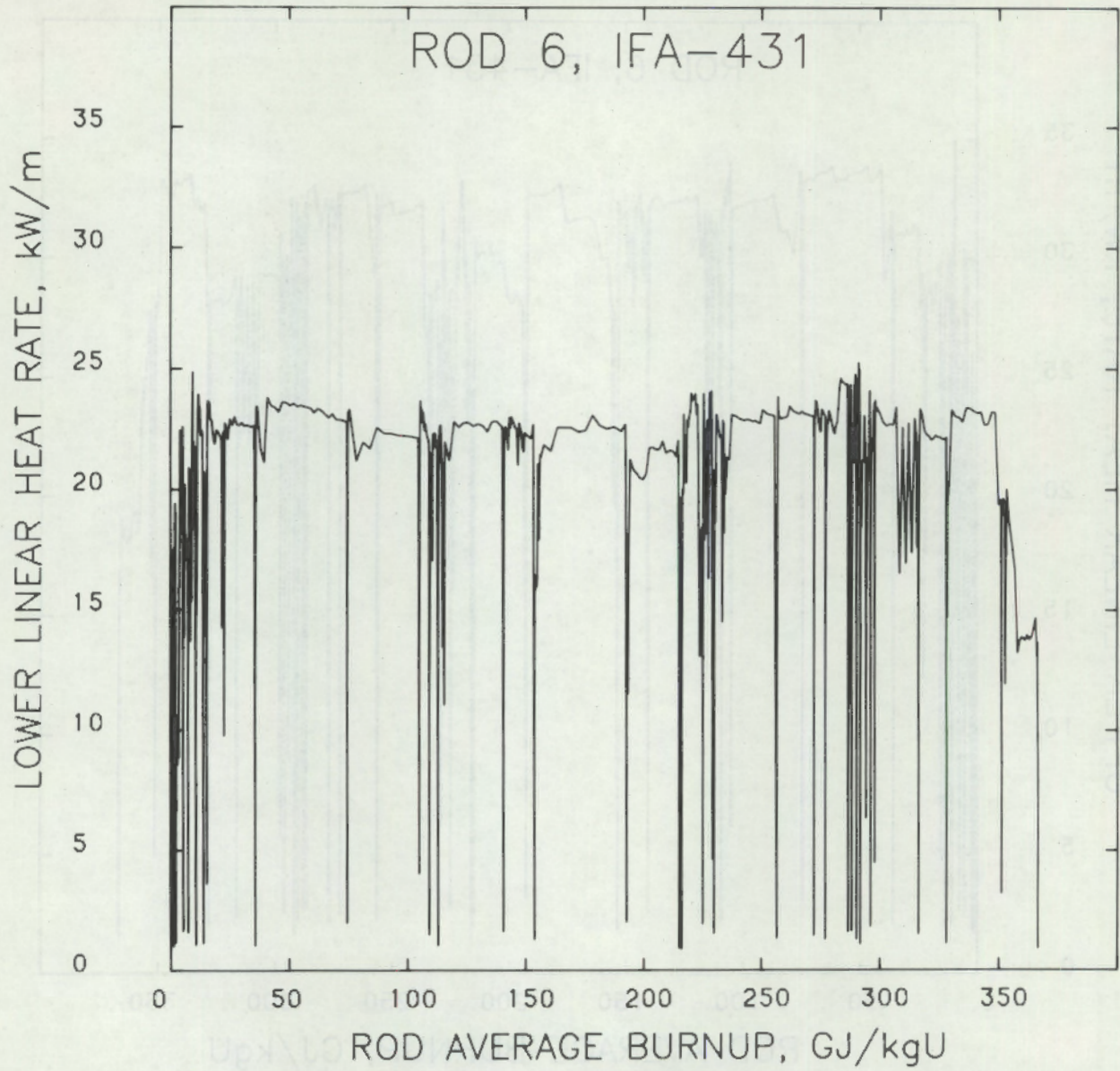
FIGURE 4. Lower Linear Heat Rate for Rod 6 of IFA-431
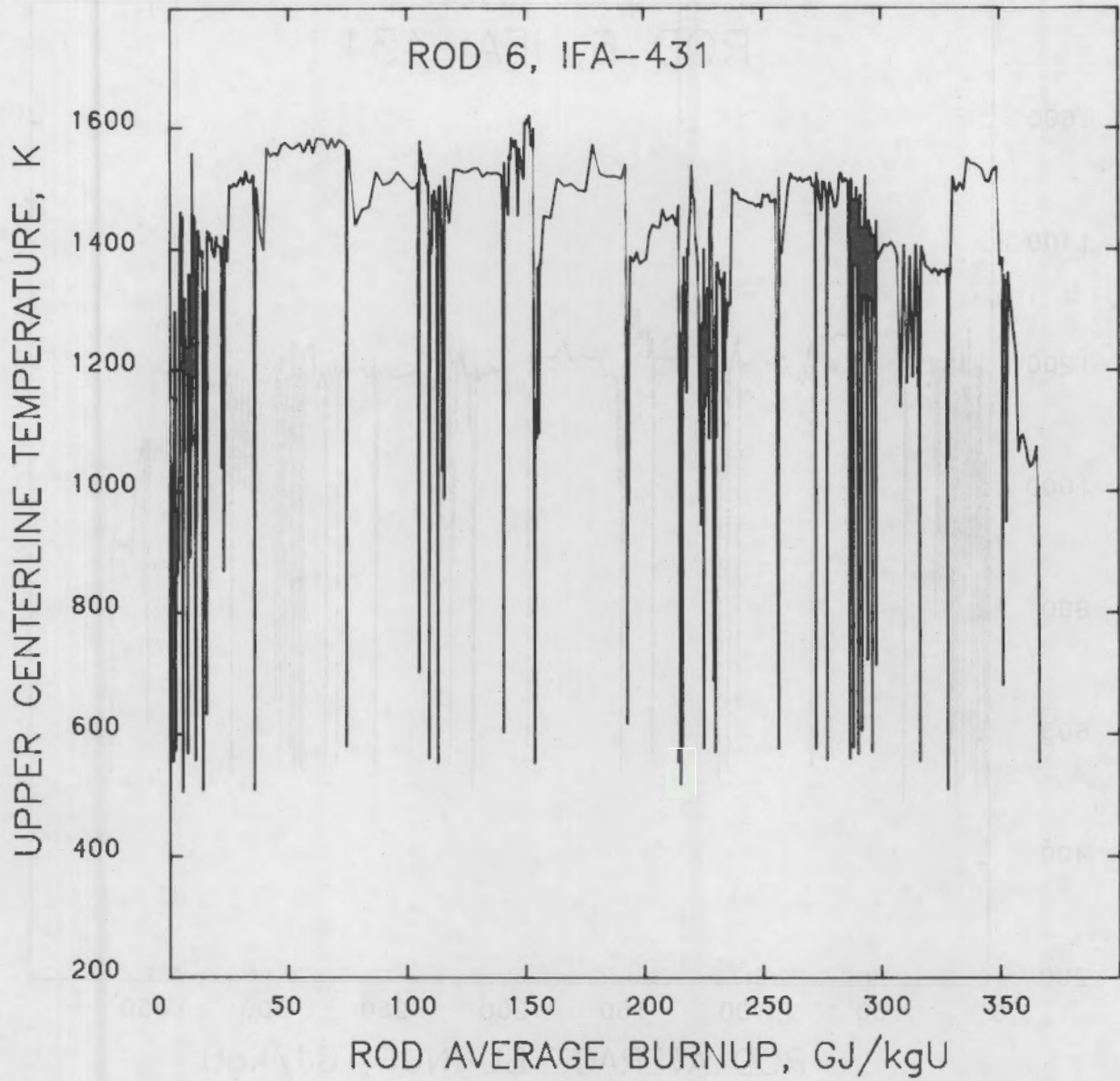
FIGURE 5. Upper Centerline Temperature for Rod 6 of IFA-431

11
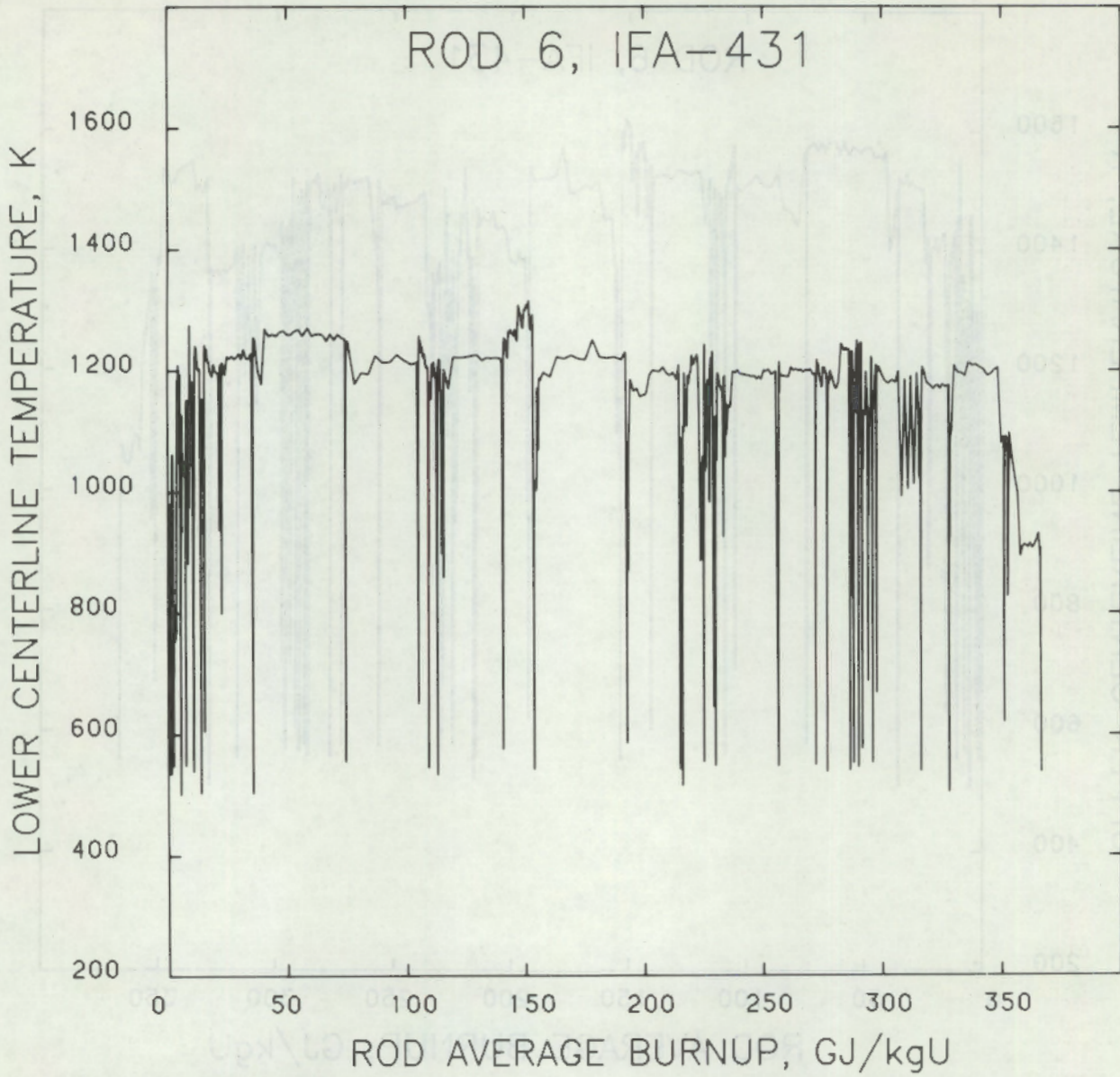
FIGURE 6. Lower Centerline Temperature for Rod 6 of IFA-431

where R_T = total thermal resistance, m-K/W

   T_{CL} = fuel centerline temperature, K

   T_W = coolant temperature, K

   LHR = local linear heat rate, kW/m.

Defined in this manner, thermal resistance is sensitive to changes in the thermal response of a fuel rod. A more extensive discussion of thermal resistance can be found in Reference 13.

ROD 6 RESISTANCE VERSUS BURNUP

Figure 7 presents the thermal resistance of rod 6 at the upper and lower thermocouple positions as a function of rod average burnup. Three principal regions are of interest in this figure. First, the resistance increased approximately 19% (from 0.026 to 0.031 m-K/W) during the first 4 GJ/kgU and was followed by another 6% increase (from 0.031 to 0.033 m-K/W) during the following 39 GJ/kgU. Second, the resistance after the 3-month shutdown (215 GJ/kgU) was approximately 5% lower than it was before the shutdown. Third, an approximately step increase in resistance from 141 to 153 GJ/kgU was followed by a return to preceding values.

A preliminary analysis might attribute the beginning-of-life (BOL) resistance increase entirely to densification; however, a closer examination indicates that densification may not have occurred immediately. The general resistance behavior of rods 6, 1 (standard rod), and 3 (small-gap, high-gap conductance) over the first 14 days at power (shutdown time is not included) is compared in Figure 8.[a] The behavior is the same for all three rods for approximately the first 8 days. Since the fuel in rods 1 and 3 was expected to have minimal densification, this initial resistance change is attributed to fuel cracking and related effects. Additionally, fuel centerline temperatures for rod 6 during this period ranged from 1025 to 1675K (750 to 1400°C), with the peak temperatures occurring for only approximately 36 h. Since the fuel

_____

(a) The initial resistance differences among the three rods are due to design differences: Rod 3 has the smallest gap and thus the lowest resistance; although rods 1 and 6 have the same gap, the fuel in rod 6 has a higher porosity and therefore lower thermal conductivity.[12]
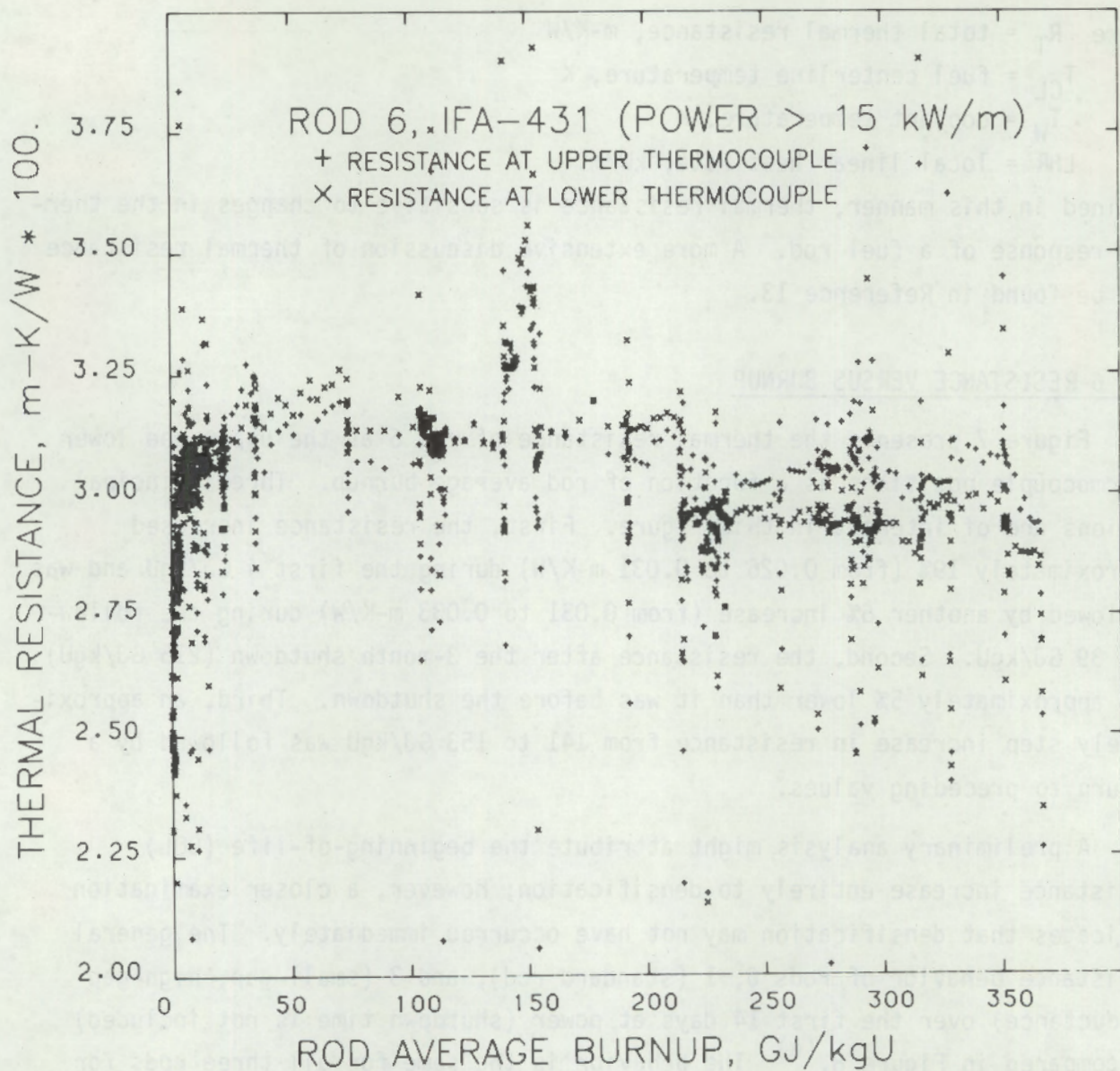
FIGURE 7. Resistance Versus Rod Average Burnup for Rod 6 of IFA-431

was initially sintered at 1973K for 8 h, this lower temperature may have been insufficient for additional sintering and densification.

After 8 days at power, the resistance of rod 6 began increasing while the resistance of rods 1 and 3 remained constant. Measured centerline temperatures during this period were greater than 1700K for 3.5 days and greater than 1800K for the last 2.5 days (see Figure 8). This resistance increase is attributed to densification of the fuel in rod 6.

14
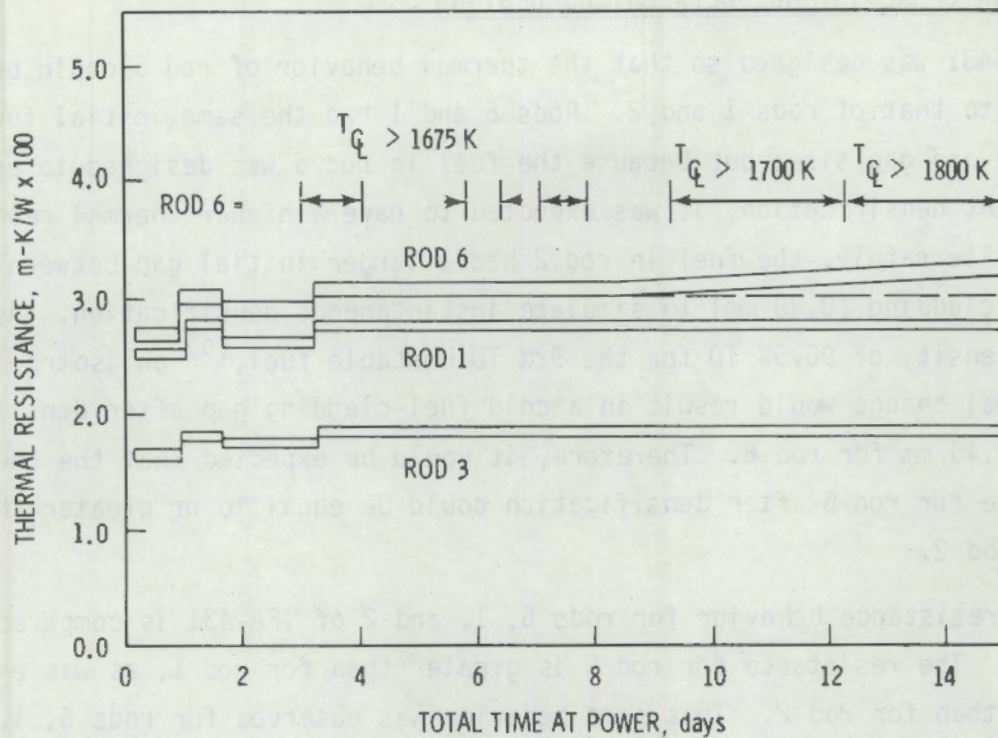
FIGURE 8. General Resistance Behavior for Rods 6, 1, and 3
of IFA-431 During Early Irradiation

The 5% drop in resistance after the extended shutdown (Figure 7) was also
observed in the other rods of IFA-431 and is believed to be due to settling of
the fuel pellet fragments, which then resulted in a reduction of the effective
fuel-cladding gap and the thermal resistance. The rise in resistance seen
during the burnup span from 141 to 153 GJ/kgU is believed to be an instrumen-
tation error. No physical reasons for such a resistance spike are suspected,
and the other rods in IFA-431 showed similar resistance spikes during the same
time period along with indications of anomalous instrumentation behavior.

The observed increase in thermal resistance for rod 6 should be princi-
pally attributed to densification and not fission gas release. Pressure mea-
surements during the irradiation indicated low fission gas release, and PIE
measurements confirmed this. The final gas mixture for rod 6 was approximately
85% helium, 10% nitrogen and carbon monoxide, and 5% fission gas.

15

COMPARISON OF RESISTANCE BETWEEN ROD DESIGNS

IFA-431 was designed so that the thermal behavior of rod 6 could be compared to that of rods 1 and 2. Rods 6 and 1 had the same initial fuel diameters and gap size; but because the fuel in rod 6 was designed to undergo significant densification, it was expected to have a higher thermal resistance. Alternately, the fuel in rod 2 had a larger initial gap between the fuel and cladding (0.38 mm) to simulate instantaneous densification. Assuming a final density of 96.5% TD for the 92% TD unstable fuel,[a] an isotropic dimensional change would result in a cold fuel-cladding gap after densification of 0.40 mm for rod 6. Therefore, it would be expected that the thermal resistance for rod 6 after densification could be equal to or greater than that of rod 2.

The resistance behavior for rods 6, 1, and 2 of IFA-431 is compared in Figure 9. The resistance for rod 6 is greater than for rod 1, as was expected, but less than for rod 2. This same behavior was observed for rods 6, 1, and 2 of IFA-432 as is shown in Figure 10. One point of concern involves the initial resistance data. As stated earlier, densification does require time and temperature and the initial resistance differences observed in Figures 9 and 10 are basically due to design differences. This is further illustrated in Figure 11, where centerline temperature as a function of power is plotted for the first rise to power. Rod 2 has the largest fuel-cladding gap and the highest centerline temperature. Rods 6 and 1 have the same gap; the lower density in rod 6 is principally responsible for its higher temperature.

By comparing the resistance behavior of rods 6, 1, and 2 and recalling that the observed total thermal resistance is dependent on densification, fuel cracking and relocation, and other factors, it can be concluded that densification does increase fuel temperatures. However, the observed temperature increase due to densification (rod 6) was less than if instantaneous densification and isotropic shrinking had occurred.

(a) Final density for rod 6 of IFA-431 fuel was measured at 96 ±1% TD.[11]
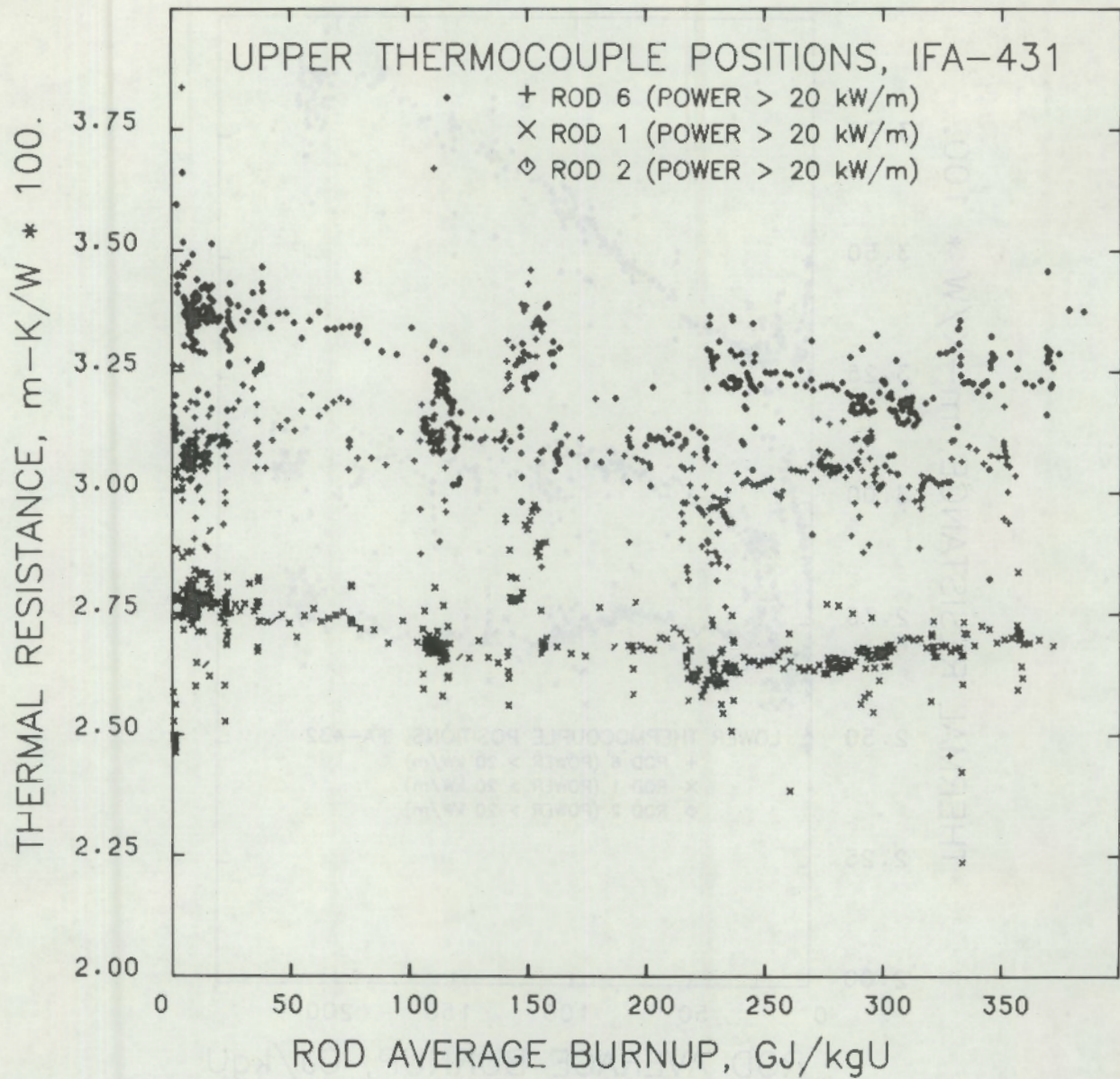
FIGURE 9. Comparison of Resistance for Rods 6, 1, and 2 of IFA-431

17
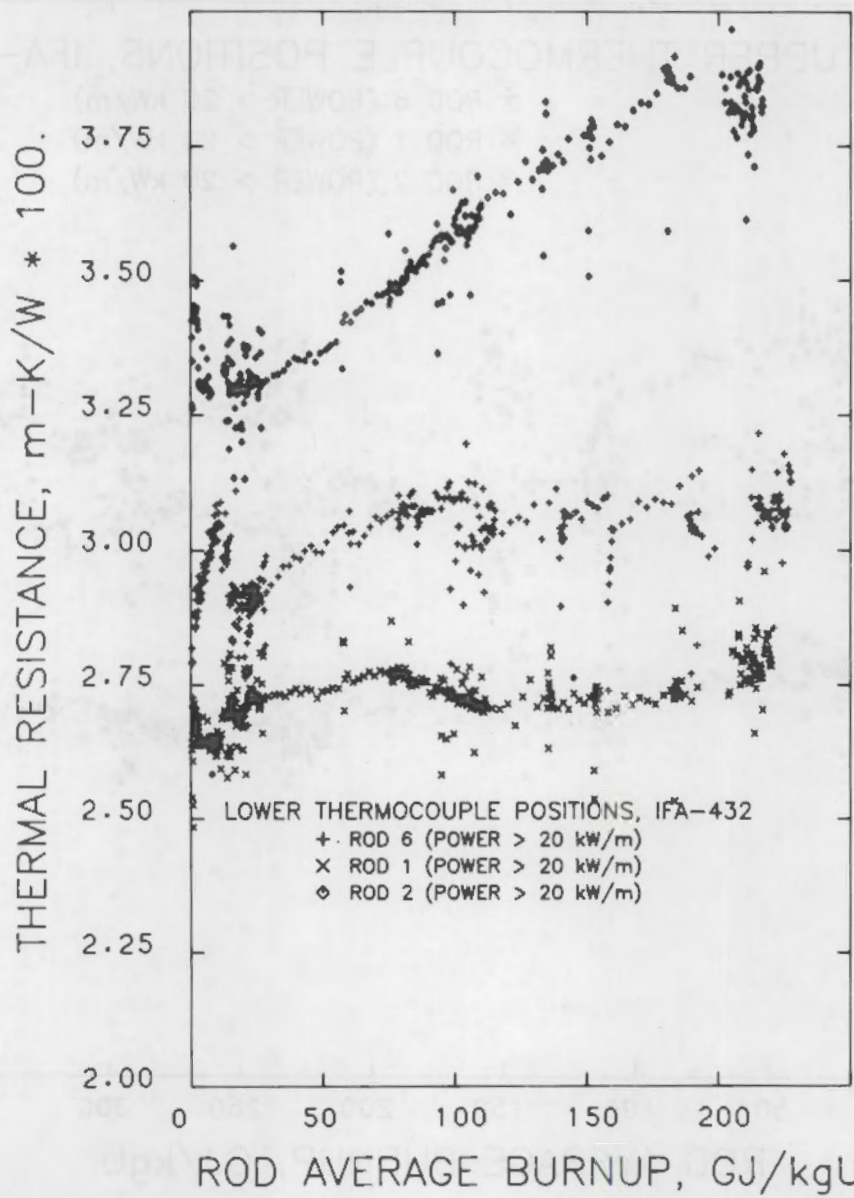
FIGURE 10. Comparison of Resistance for Rods 6, 1, and 2 of IFA-432
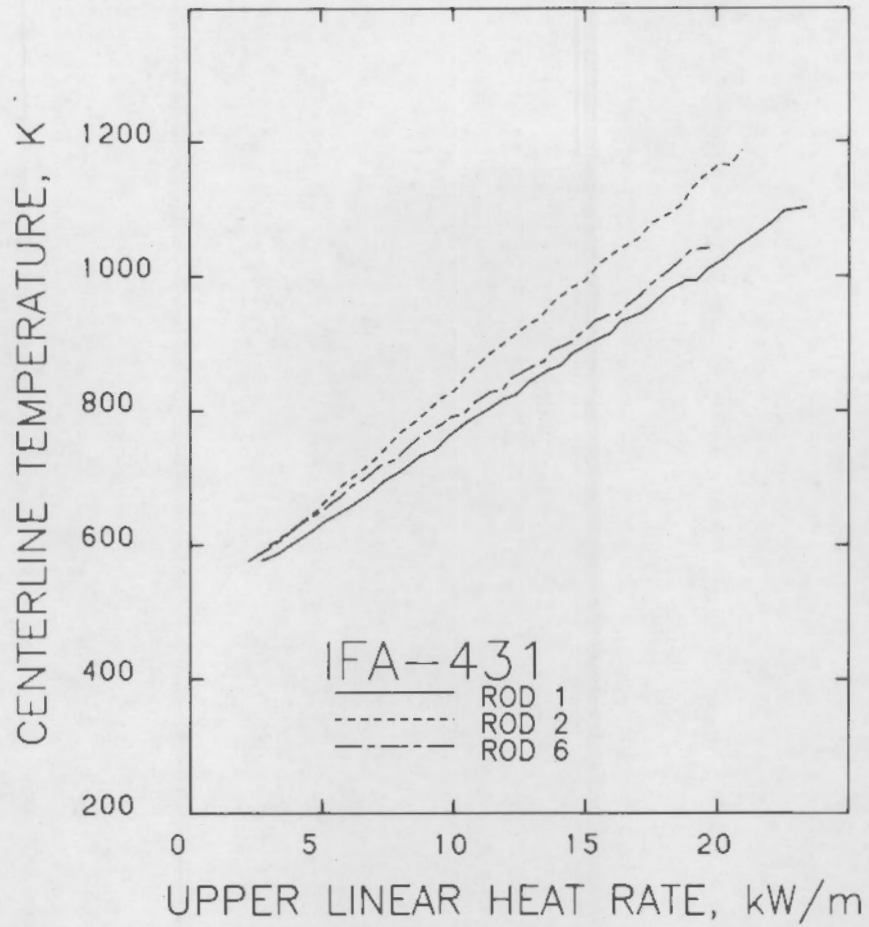
FIGURE 11. Centerline Temperature as a Function of
Power During First Power Ascension

FIGURE 11. Centerline Temperature as a Function of
Power During First Power Ascension

UPPER LINEAR HEAT RATE, kW/m

CENTERLINE TEMPERATURE, K

MICROSTRUCTURAL ANALYSIS

PURPOSE AND GENERAL PROCEDURE

Microstructural analysis of pellets 13 and 39 of rod 6 of IFA-431 was conducted to compare the pre- and postirradiated structures and evaluate the effects of irradiation on unstable fuel. Of particular interest were the changes in porosity and grain size, which are especially significant relative to densification behavior.

The analysis was conducted as a cooperative effort by PNL and Harwell. At PNL, detailed precharacterization of sibling pellets of this fuel type was conducted as reported in Reference 12. That work included high-resolution metallography, optical and scanning electron microscopy, quantitative image analysis of porosity, and estimation of grain size. From this data the characteristics of inherent porosity and the propensity for densification were determined. At Harwell, metallography and microscopy were conducted on an as-sintered sibling archive pellet to demonstrate that Harwell specimen preparation, metallography, and microscopy procedures to be applied to the irradiated pellets were comparable. The Harwell micrographs were quantitatively analyzed at PNL using the same procedures as for the PNL preirradiation characterization work. The procedures generally followed the methods outlined in Reference 12.

In this report, the qualitative results of metallography and representative illustrations of microstructure obtained both in precharacterization and PIE work are presented and provide a visual comparison of the fuel materials. Quantitative data from image analysis of those microstructures is presented, and the pre- and postirradiation comparisons are summarized.

MICROSCOPY

Microscopy was conducted on polished sections of pellets prepared by standard metallography techniques. PNL precharacterization work was conducted on two randomly selected pellets of this unstable fuel type that were sectioned transversely and longitudinally for microscopy. At Harwell, metallography on

21

archive and irradiated pellets was conducted on transverse sections only. Figure 12 shows the polished sections of as-sintered pellets at low magnification; the locations of the subsequent high-magnification photomicrography are indicated. Similarly, the cross sections of the irradiated pellets examined are shown in Figure 13. The sites for subsequent detailed porosity studies include a representative sampling of peripheral, midradius, and center locations. This procedure permits identification of any differences in densification or pore size distribution relative to radial locations in each pellet and allows verification that the as-sintered pellets were homogeneous. Observed qualitative differences between as-sintered and irradiated fuel are illustrated in Figure 14. There are significantly fewer pores present after irradiation, which is typical of densification.

Examples of more detailed preirradiation microscopy conducted at PNL and Harwell are compared in Figures 15 and 16. Both of these figures show a significant number of small pores (visible at the higher magnification) as well as a uniform distribution of larger pores. Some difficulties were initially experienced at the Harwell laboratory with pull-out from the pellet surface during polishing; and although these problems were largely overcome by a modified polishing method, the equipment that was utilized was unable to provide as sharp a definition of pores at the higher magnification as in the PNL series. However, qualitatively, the two sets of micrographs are comparable.

The microscopy conducted on the two irradiated pellets is illustrated in Figures 17 and 18. As mentioned previously, irradiation tended to densify the pellets, resulting in fewer pores. The lower burnup pellet (39) shows the initial stage of a grain boundary concentration of pores; the higher burnup pellet (13) contains a pronounced concentration of pores in the grain boundaries (in the axial regions in particular where the temperature was the highest). Grain definition is also enhanced in both of these irradiated pellets and particularly in pellet 13.

Grain size measurements were conducted on etched surfaces of the same pre- and postirradiation pellets. Figure 19 shows the preirradiation condition observed at PNL and Harwell. In the PNL precharacterization, the grains are

TRANSVERSE
SECTION

LONGITUDINAL SECTION
AS-SINTERED PELLET (PNL)

⌞__⌟
1 mm

-A-

-M-

-P-

TRANSVERSE SECTION

—AXIAL

—MIDRADIUS

—PERIPHERAL

AS-SINTERED ARCHIVE PELLET (HARWELL)   ⌞__⌟ 1 mm
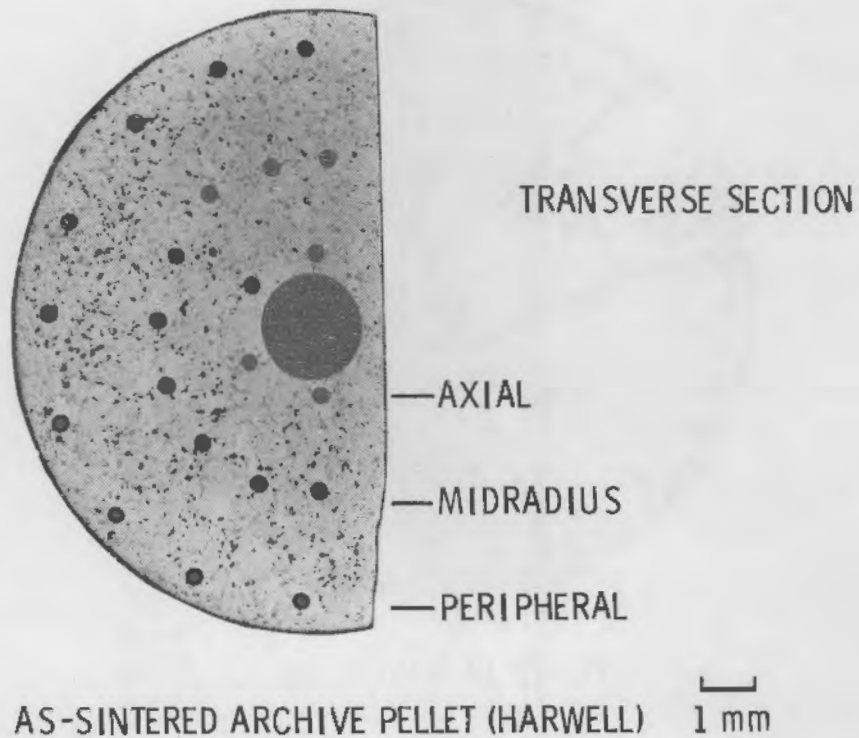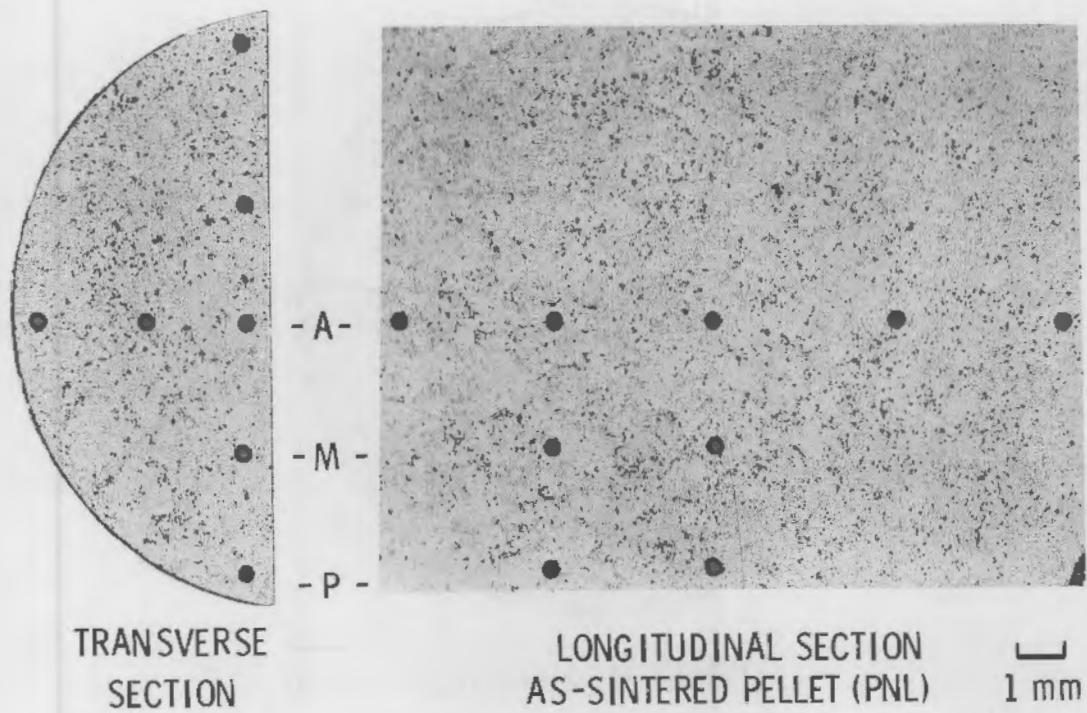
FIGURE 12. Polished Sections of 92% TD As-Sintered Pellets Used for Rod 6
of IFA-431. Locations of photomicrography for study of
porosity, microstructure, and grain size are shown.

23
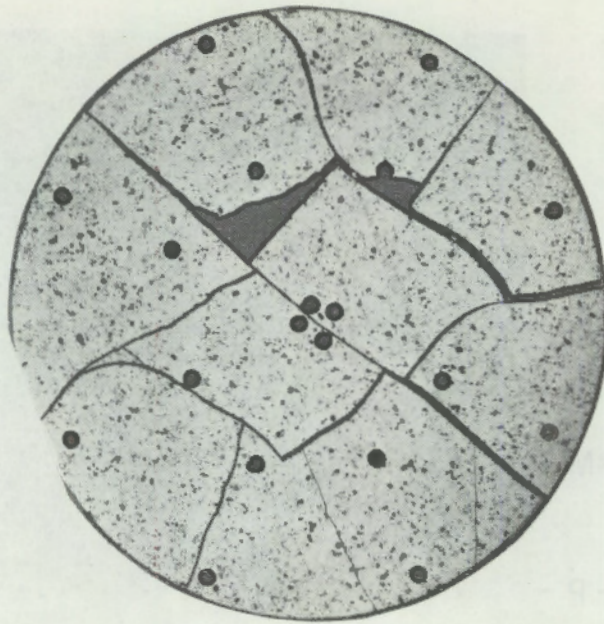
PELLET 39 (HARWELL)   1 mm
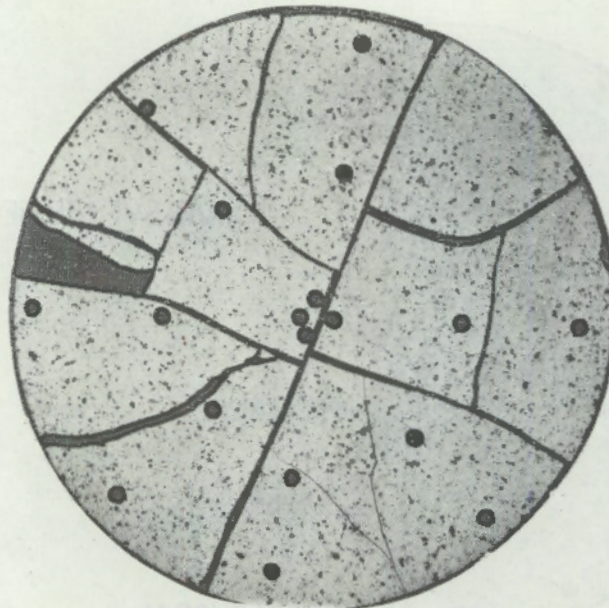
PELLET 13 (HARWELL)   1 mm

FIGURE 13. Polished Sections of 92% TD Irradiated Pellets Used for Rod 6 of IFA-431. Locations of photomicrography for study of porosity, microstructure, and grain size are shown.
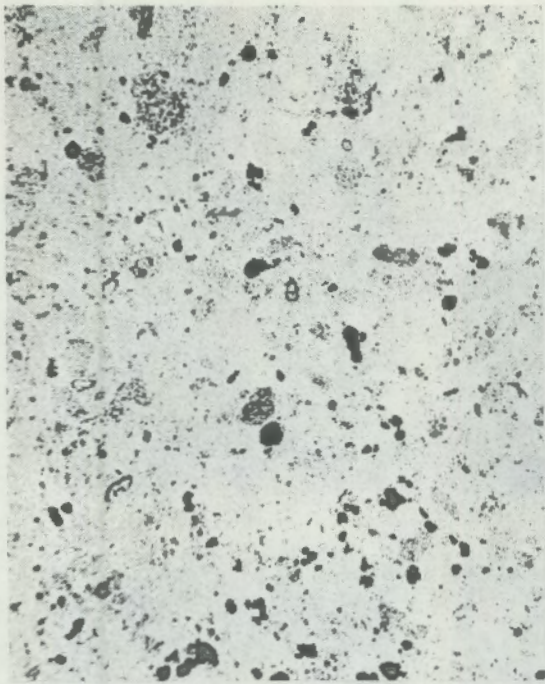
PRECHARACTERIZATION (PNL)   ARCHIVE PELLET (HARWELL)
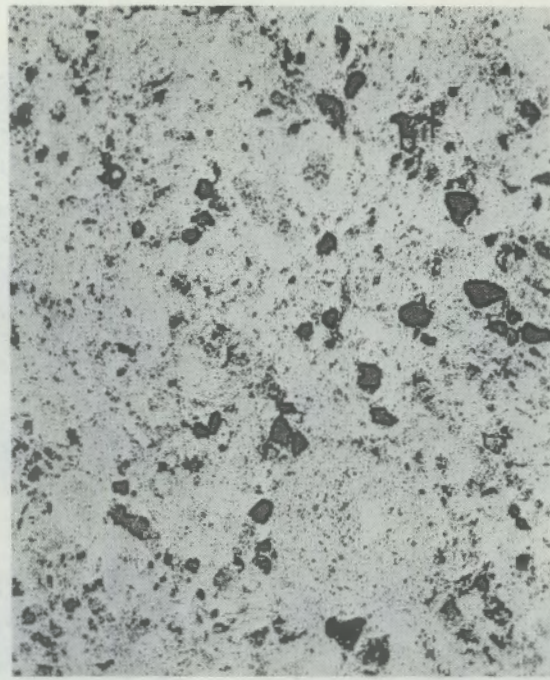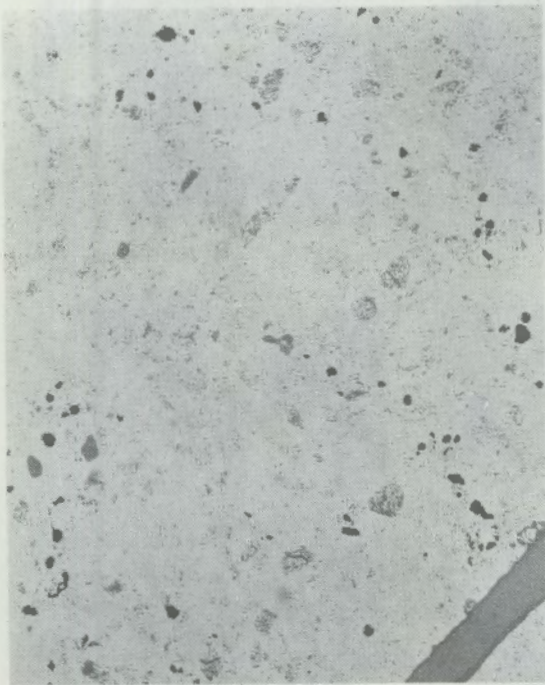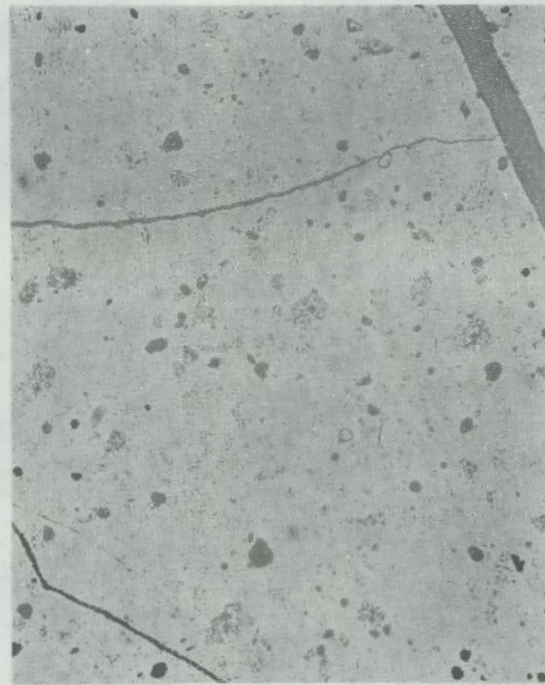
IRRADIATED PELLET 39   IRRADIATED PELLET 13   ⊢——⊣ 200 μm

FIGURE 14. Comparison of Polished Sections of As-Sintered
and Irradiated Pellets of 92% TD Fuel

50 μm

5 μm

PERIPHERY   MIDRADIUS   AXIS

1 μm
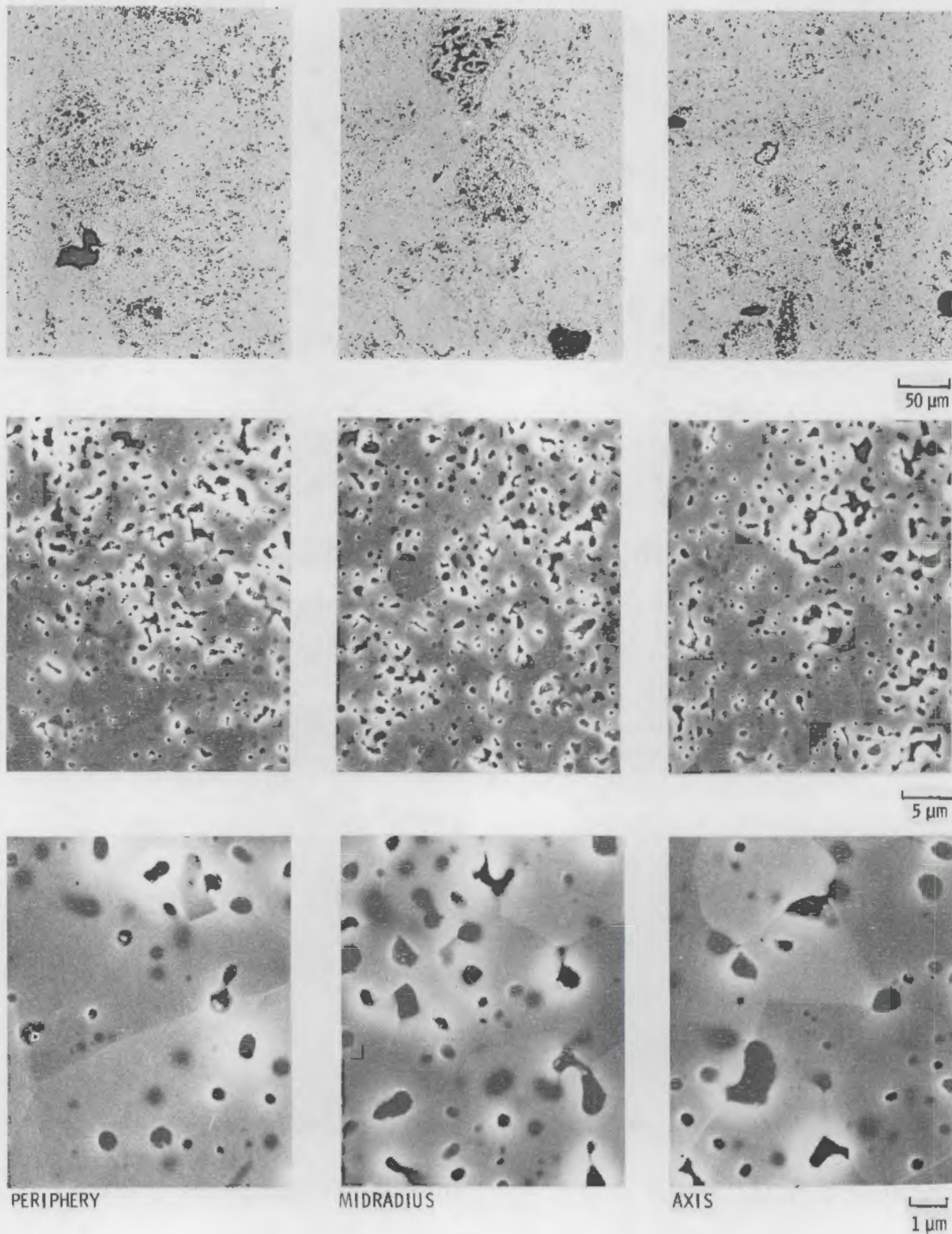
FIGURE 15.   Typical Radial Distribution of Porosity of 92% TD
              As-Sintered Fuel (polished sections)

26

PERIPHERY   MIDRADIUS   AXIS
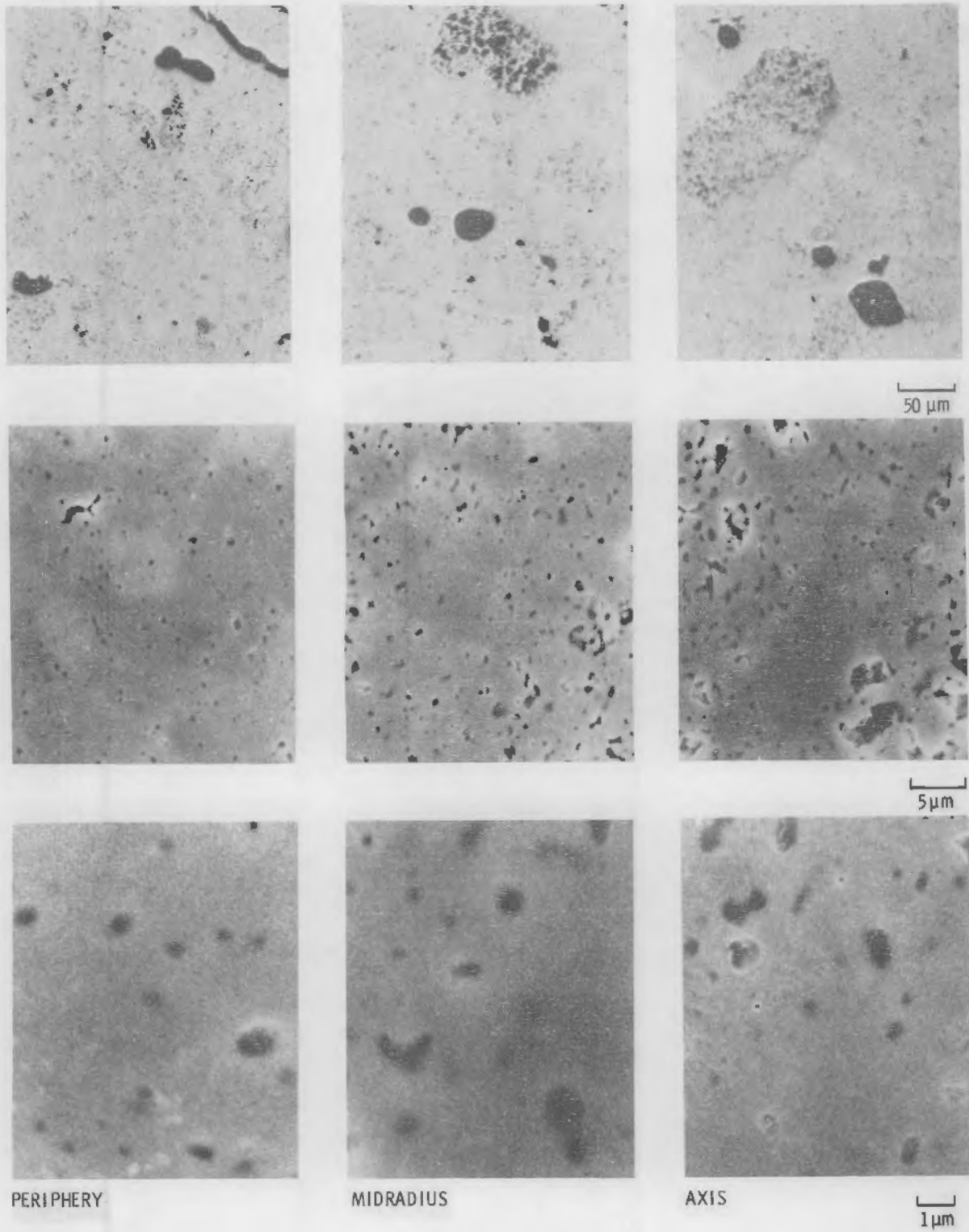
FIGURE 16. Typical Radial Distribution of Porosity of 92% TD As-Sintered
Harwell Archive Fuel Pellet (polished sections)

27

PERIPHERY   MIDRADIUS   AXIS
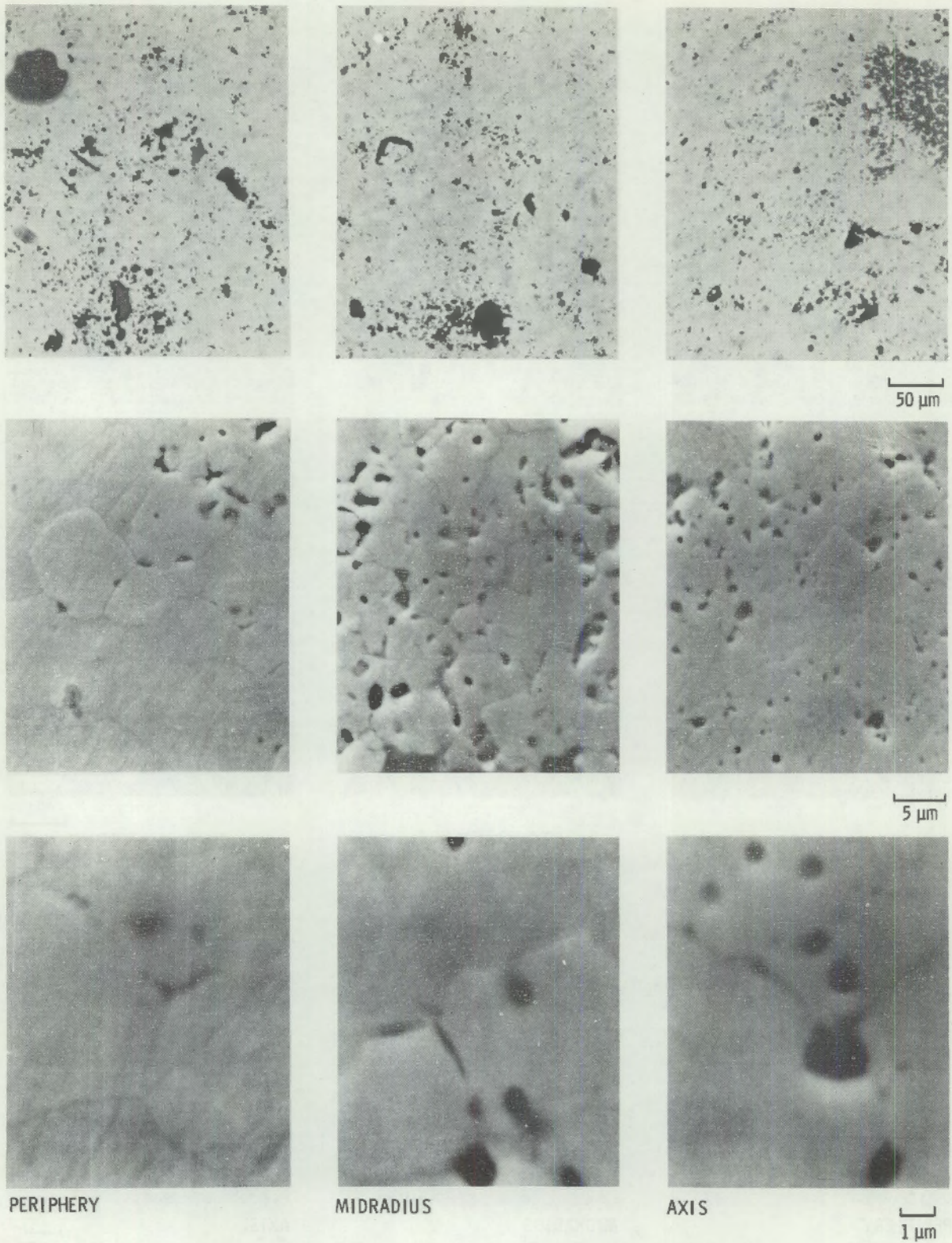
FIGURE 17. Typical Radial Distribution of Porosity of Irradiated
Pellet 39 of Rod 6 of IFA-431 (polished sections)

28

PERIPEHRY   MIDRADIUS   AXIS
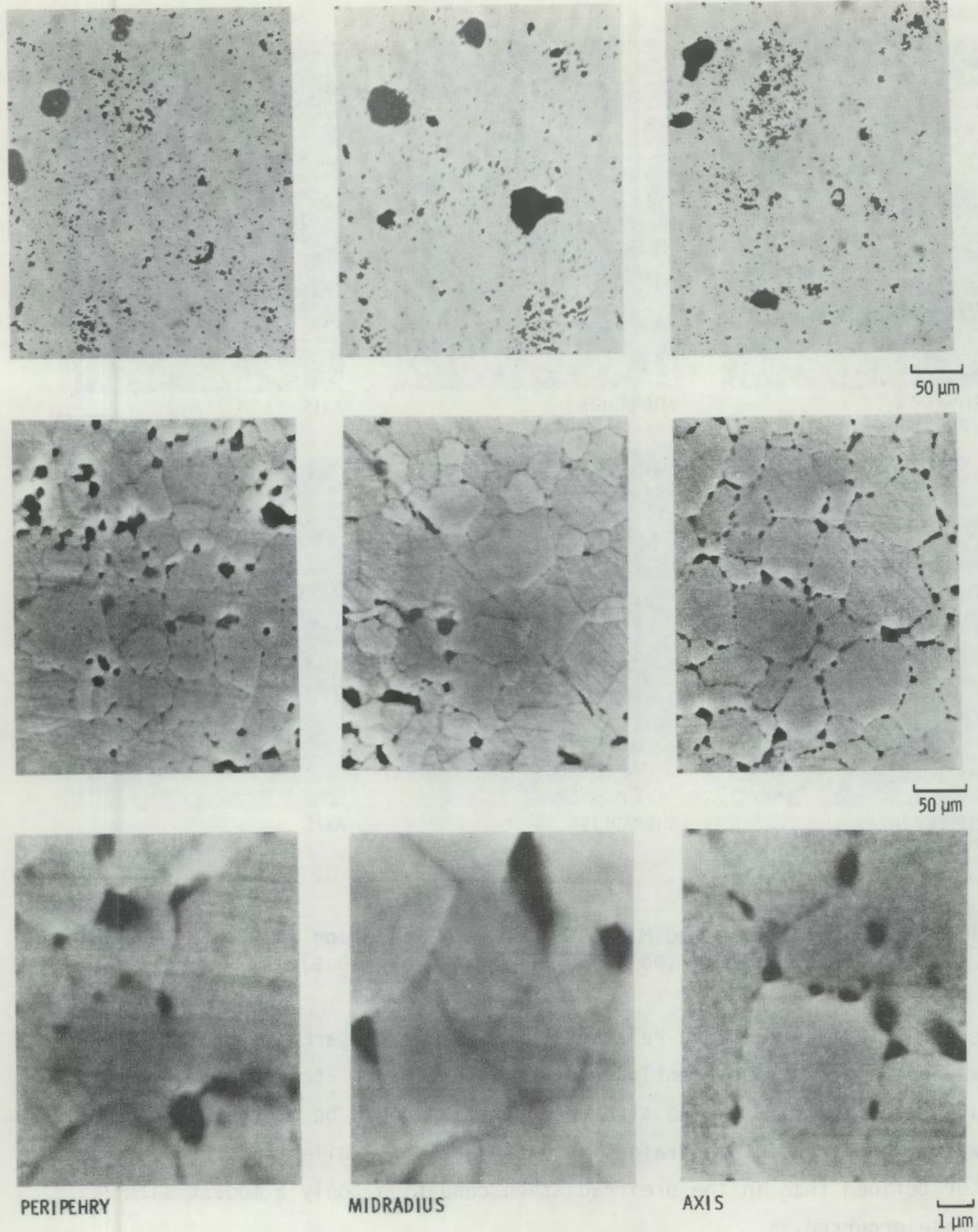
FIGURE 18. Typical Radial Distribution of Porosity of Irradiated
Pellet 13 of Rod 6 of IFA-431 (polished sections)

29
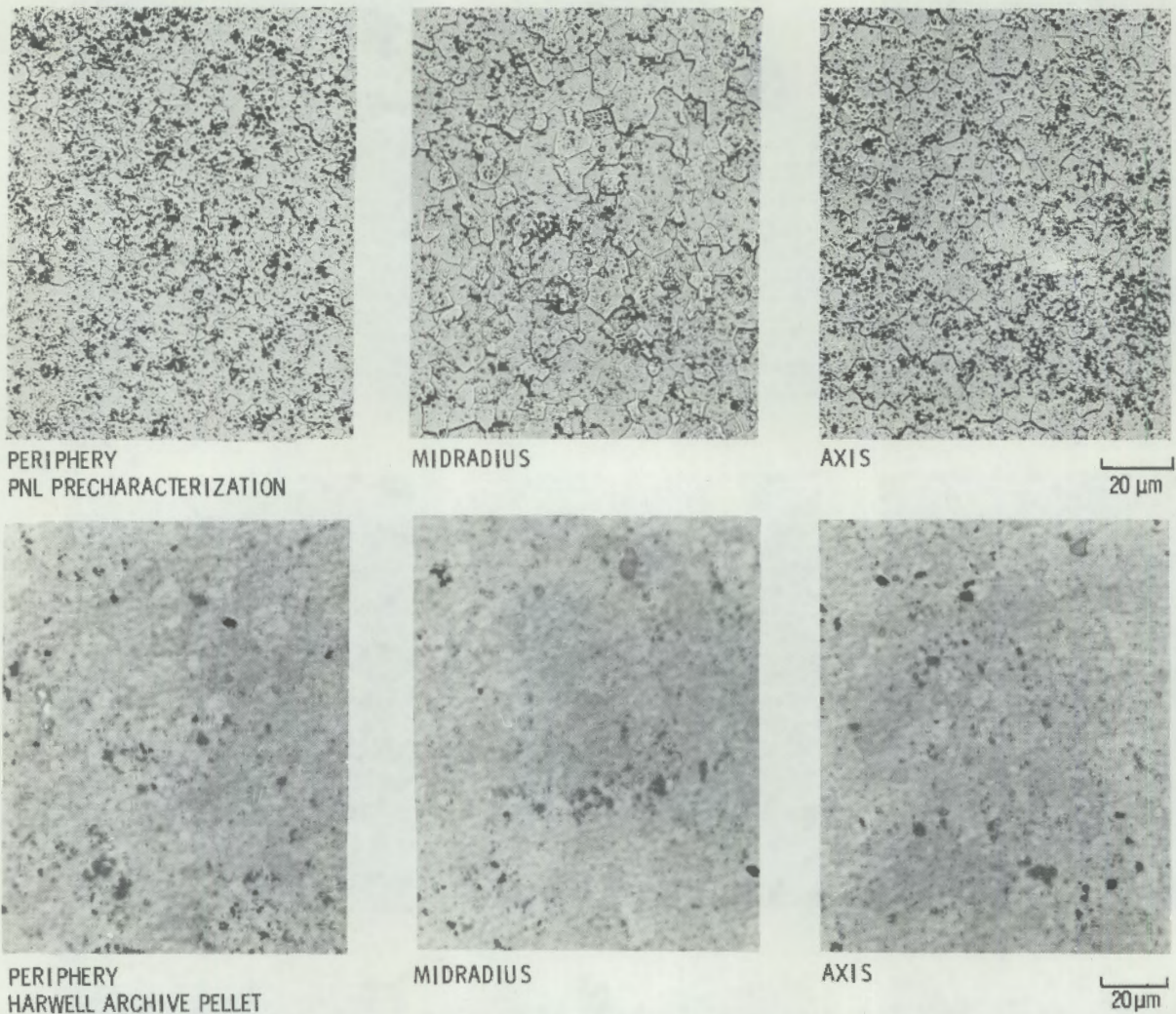
FIGURE 19. Grain Size and Microstructure Distribution in 92% TD As-Sintered
Fuel Pellets (polished and etched sections)

reasonably well defined and relatively small. In the archive pellet from
Harwell, the pellets apparently received insufficient etching to define the
grains satisfactorily and no size determination could be made. Figure 20
shows the postirradiation grain size distribution. While the grains are much
better defined than in the preirradiation condition, only a modest size
increase occurred.

PERIPHERY
PELLET 39

MIDRADIUS

AXIS

20 µm

PERIPHERY
PELLET 13

MIDRADIUS

AXIS

20 µm
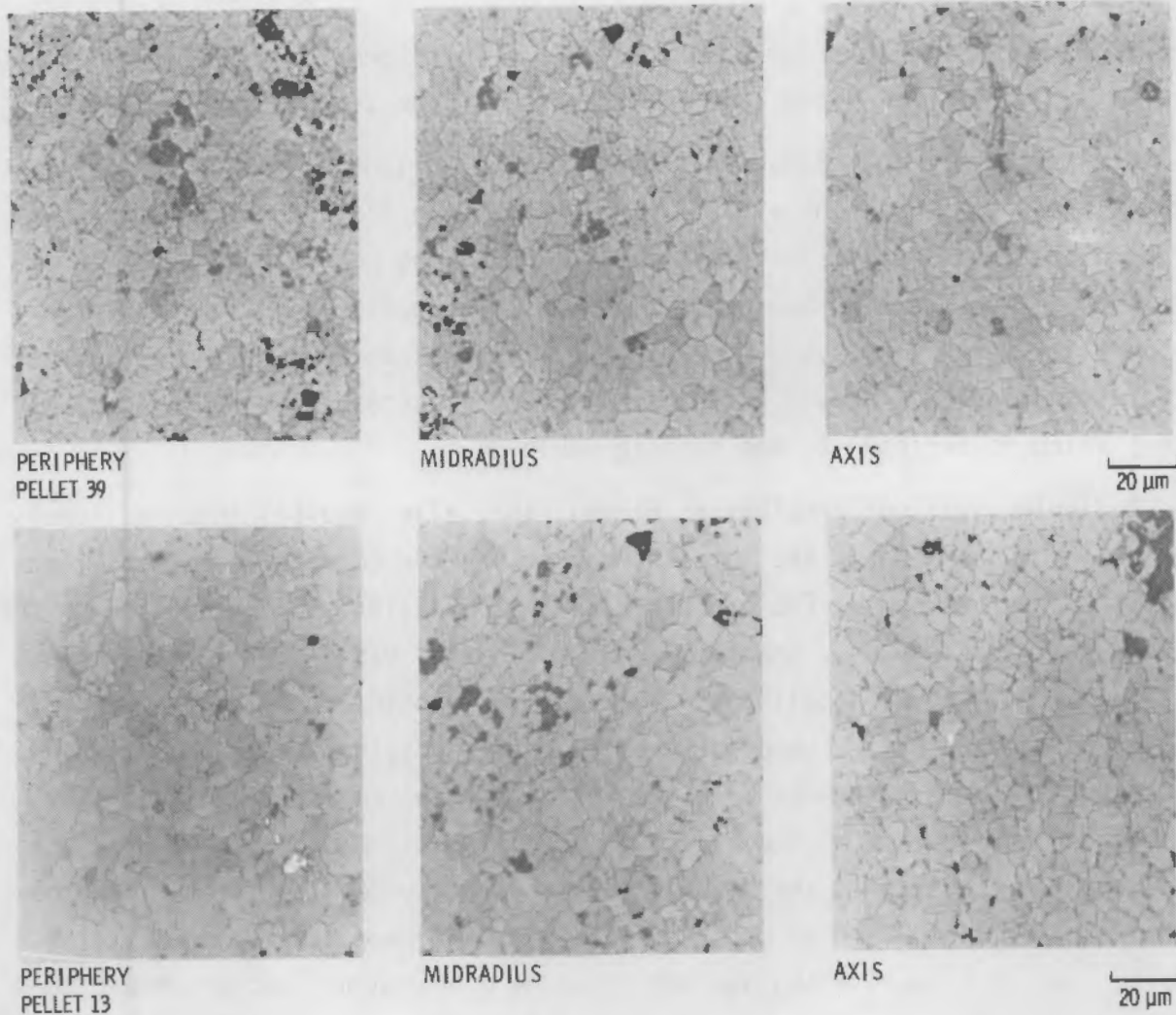
FIGURE 20. Grain Size and Microstructure Distribution in Irradiated Pellets
from Rod 6 of IFA-431 (polished and etched sections)

QUANTITATIVE MICROSTRUCTURAL ANALYSIS

The quantitative examination and measurement of all photomicrographs were
conducted using a quantitative image analyzer (Quantimet-720) in the manner
described in Reference 12. In this method, each pore in the polished section
is examined, its diameter is automatically measured, and these measurements
are distributed into size and volume histograms. The three-dimensional volume
distribution of the pores within the body of the pellet is estimated from the
data using a special computer program (LINEST-II). The assumption is made

31

that these pores are spherical and that they are uniformly distributed throughout the pellet volume in the same manner observed for the polished section.

The preirradiation characterizations of fuel pellets examined at PNL and Harwell are compared in Table 3. PNL and Harwell photomicrographs were analyzed on the quantitative image analyzer at PNL. The PNL data showed good agreement between density measurements (made by standard immersion methods) and porosity measurements. Since this fuel type was deliberately prepared as a densifying fuel, it should contain an appreciable fraction of <1-μm diameter pores, which is verified by the data in Table 3.

Polishing pull-out problems at Harwell initially resulted in an extremely high pore volume although the total number of pores observed was actually less than that observed in the PNL precharacterization pellet. Upon repolishing the archive pellet at Harwell, the total volume observed was slightly lower than the nominal 8 to 9%; and pull-out was largely eliminated. Low volume was due largely to the apparent absence of submicrometer porosity; other pore size ranges were in good agreement with the PNL data. The relatively high median pore diameter results from the apparent lack of submicrometer pores. The low submicrometer porosity in the Harwell data apparently resulted from a combination of the polishing method used and inadequate microscope resolution. Subsequent work at Harwell using another scanning electron microscope showed a frequency of submicrometer pores in qualitative agreement with PNL data.

Table 4 shows the effects of irradiation on the porosity characteristics of the fuel pellets from rod 6, based on image analysis of photomicrographs of the type illustrated in Figures 17 and 18. While the PNL preirradiation immersion density measurements agreed well with the corresponding pore volume measurements, the Harwell postirradiation immersion density of adjacent pellet 40 does not agree with the Quantimet porosity calculations made on pellet 39. However, there is good agreement between the porosity measurements by photomicrographs of pellet 13 and the postirradiation immersion density of adjacent pellet 12. From previous experience at PNL on a variety of fuel materials, it is concluded that quantitative porosity data and the volume of pores determined therefrom are likely to be the better measurements of the density changes that take place throughout the pellet.

32

TABLE 3. Comparison of Preirradiation Characterization of Typical 92% TD Fuel Pellets at PNL and Harwell[a]

	PNL Reference Pellet[b]	Harwell Archive Pellet[c]	
Porosity Volume, %	Pellet 1-6-457	First Polish	Second Polish
By Density Measurement	8.7	NA[d]	NA
By Pore Measurement	9.1 $\pm$0.3	20.4 $\pm$0.7	6.8 $\pm$0.8
Pores <1 μm	3.5	3.8	1.3
Pores >1 μm	5.6 $\pm$0.3	16.6 $\pm$0.7	5.5 $\pm$0.8
Pores >10 μm	2.7 $\pm$0.3	8.9 $\pm$0.7	2.9 $\pm$0.8
Pore Diameter, μm			
Median, all	1.8	4.8	4.8
Median, <1 μm	0.6	0.8	0.6
Median, >1 μm	8.5	24	11
Median, >10 μm	32	53	40
Maximum	220	101	127
Pore Population, no./cm^3			
All Pores	1.9 $\pm$0.1 x 10^{12}[e]	1.1 $\pm$0.2 x 10^{12}[f]	0.39 $\pm$0.04 x 10^{12}[g]
Pores >1 μm	1.2 $\pm$0.1 x 10^{10}	3.7 $\pm$0.2 x 10^{10}	0.59 $\pm$0.11 x 10^{10}
Pores >10 μm	5.6 $\pm$0.7 x 10^6	3.6 $\pm$2.0 x 10^6	5.8 $\pm$0.2 x 10^6

(a) Confidence intervals = 1σ SD, based on image analysis calculations only.
(b) All sample preparation, microscopy, and image analyses conducted on reference fuel pellet at PNL (see Reference 12).
(c) Sample preparation and microscopy of archive pellet conducted at Harwell; image analysis conducted at PNL using Harwell photomicrographs.
(d) NA = not available; nominal porosity = 8%.
(e) All pores >0.065-μm diameter.
(f) All pores >0.061-μm diameter.
(g) All pores >0.108-μm diameter.

33

TABLE 4. Effects of Irradiation on Porosity Characteristics of 92% TD Fuel Pellets from Rod 6 of IFA-431

	PNL Preirradiation[a] Characterization (Ident. No. 457)	Irradiated Pellets[a] Rod 6, Pellet 39 (Ident. No. 704)	Rod 6, Pellet 13 (Ident. No. 745)
Estimated Burnup, at.%[b]	0	0.41	0.55
Approximate Maximum Thermocouple Temperature, K	---	1223	1523
Porosity Volume, %			
By Density Measurement			
Preirradiation[c]	8.7	7.6	8.0
Postirradiation[b]	---	3.4	3.7
By Pore Measurement	9.1 ± 0.3	6.1 ± 0.3	4.1 ± 0.2
Pores <1 µm	3.5	0.5	0.5
Pores >1 µm	5.6 ± 0.3	5.6 ± 0.3	3.6 ± 0.2
Pores >10 µm	2.7 ± 0.3	2.2 ± 0.3	1.8 ± 0.2
Pore Diameter, µm			
Median, all	1.8	5.4	7.1
Median, <1 µm	0.6	0.8	0.9
Median, >1 µm	8.5	7.0	12
Median, >10 µm	32	45	45
Maximum	220	111	84
Pore Population, no./cm³			
All Pores	$1.9 \pm 0.1 \times 10^{12}$[d]	$0.14 \pm 0.04 \times 10^{12}$[e]	$0.15 \pm 0.04 \times 10^{12}$[e]
Pores >1 µm	$1.2 \pm 0.1 \times 10^{10}$	$0.69 \pm 0.05 \times 10^{10}$	$0.27 \pm 0.01 \times 10^{10}$
Pores >10 µm	$5.6 \pm 0.7 \times 10^{6}$	$5.2 \pm 2.5 \times 10^{6}$	$1.6 \pm 1.9 \times 10^{6}$

(a) Confidence intervals = 1σ SD, based on image analysis calculations only.
(b) Burnup and density of adjacent pellets 40 and 12 as measured at Harwell during PIE (see Reference 11).
(c) Immersion density measurements at PNL.
(d) All pores >0.065-µm diameter.
(e) All pores >0.070-µm diameter.

Some of the specific features shown in the table are typical of densification behavior. A decrease in the submicrometer pore volume occurs, which is at the same time reflected in the increased median pore diameter. A significant decrease is also observed in the total pore volume, accompanied by a marked decrease in the total pore population, particularly in the case of pellet 13. Comparison of the postirradiation data with the Harwell archive pellet data shown in Table 3 leads to the same conclusions although the relative differences would be somewhat smaller. It can be concluded that in-reactor densification is confirmed.

The details of the pore size and volume relationships for both pre- and postirradiation data are illustrated in Figures 21 and 22. In Figure 21, the preirradiation characterization shows a satisfactory similarity between the pellets prepared and examined at PNL and Harwell; the differences cited earlier for the total volume of submicrometer porosity are clearly indicated by the size of the peak at that end of the curve. Other components of the curves and pore volume distribution are in close agreement. In Figure 22 the differences between pre- and postirradiation curves are clearly illustrated as is the difference between pellets 13 and 39. With increasing irradiation, the total pore volume in the submicrometer range continued to decrease and the total pore volume in the midrange and larger sizes simultaneously increased. These curves are consistent with the summary data described in Tables 3 and 4.

The radial distribution of porosity in the irradiated pellets is summarized in Tables 5 and 6. Harwell measurements of immersion density using small core samples taken from the polished surface of these pellets indicated a density difference across the diameter of the pellet, but these density differences are not confirmed by quantitative image analysis. On each polished cross section, the densities calculated from pore volume are essentially the same across the entire radius. Slight densification might be indicated at the mid-radius position, but the error bars are too large to confirm that difference. There appears to be a definite trend toward fewer submicrometer pores at the center of the pellet, which is confirmed by the larger median diameter in the center and by the smaller total pore population. The largest pores are near the periphery and the smallest are at approximately midradius. The large standard deviations are due primarily to the relatively few pores present.

35
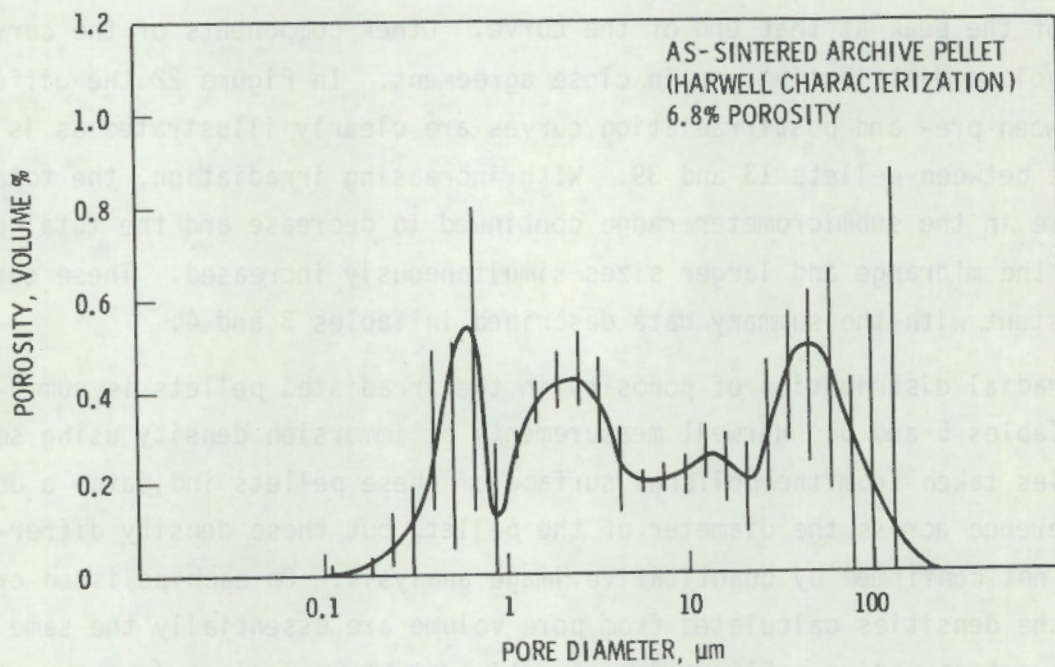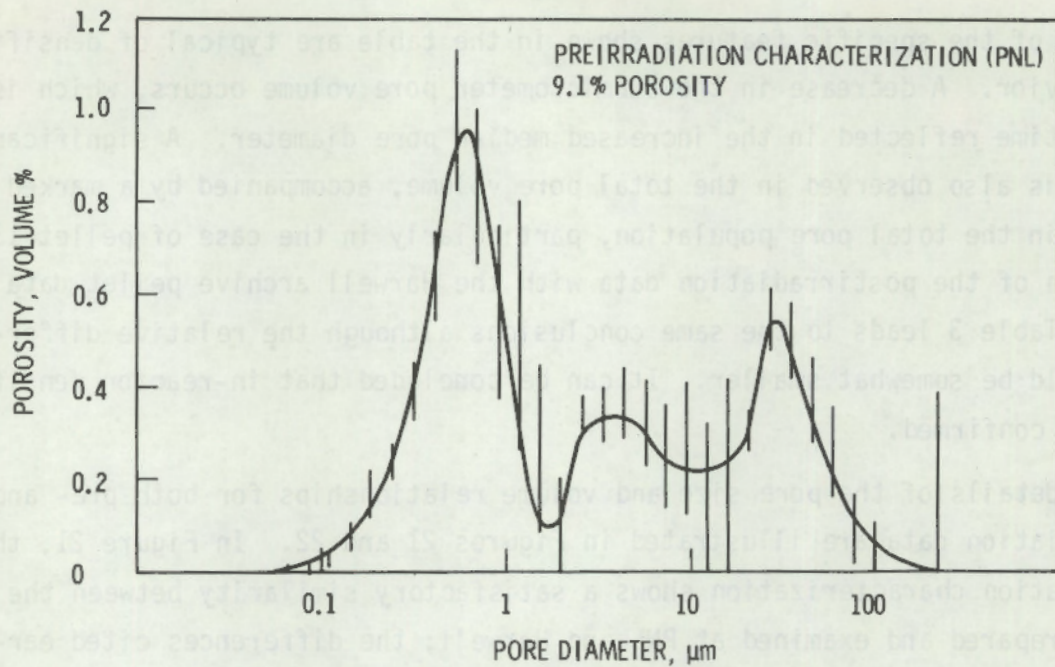
FIGURE 21. Pore Size and Volume Distribution in 92% TD As-Sintered Pellets (error bars = 2σ SD)
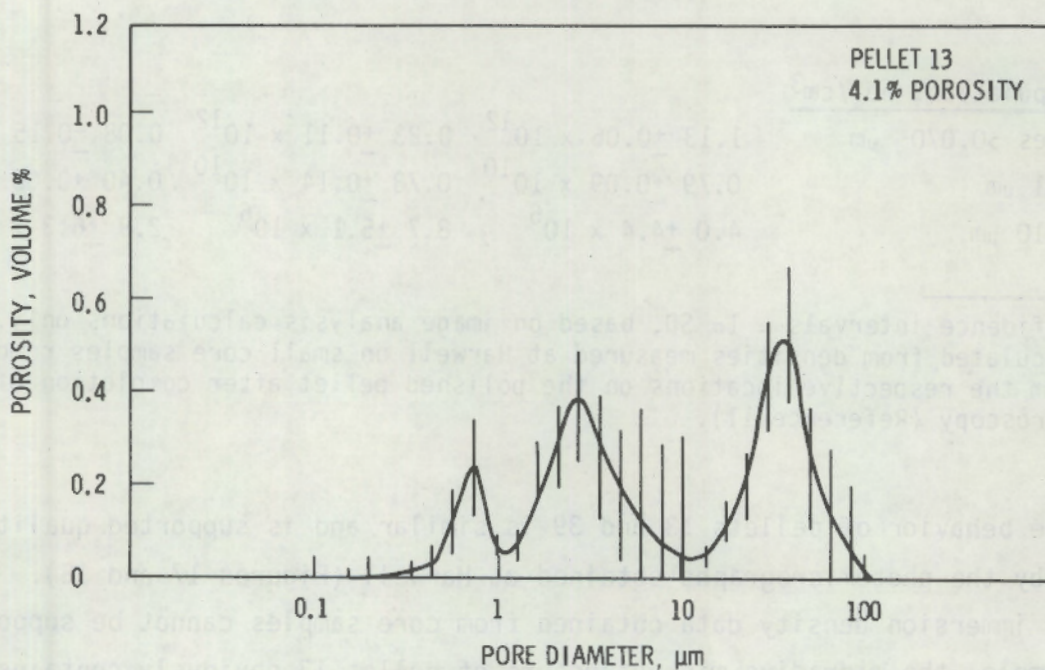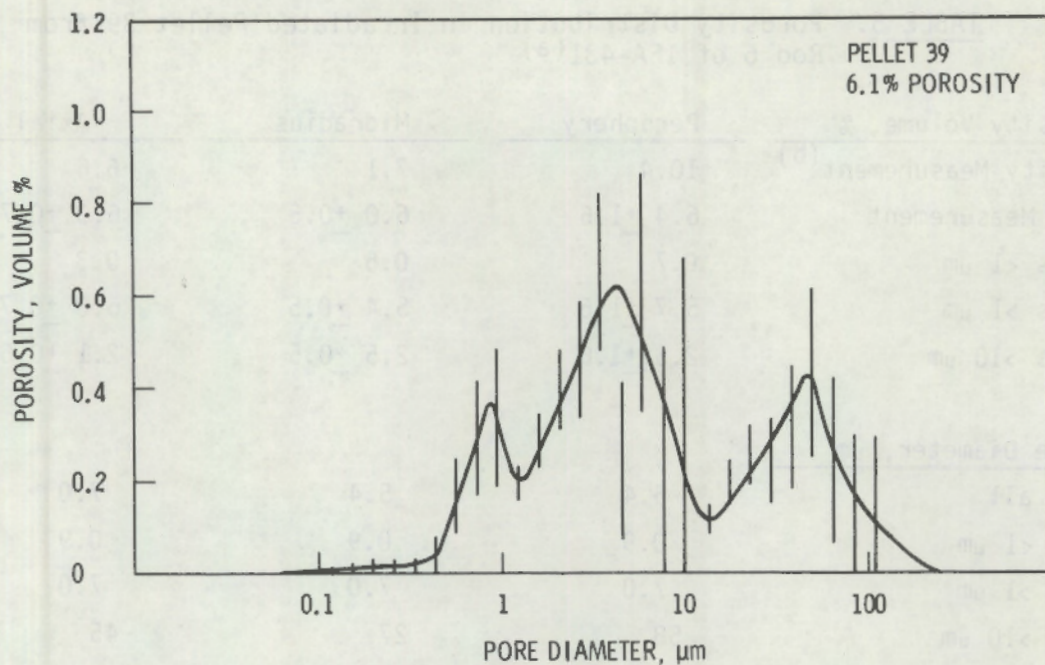
FIGURE 22. Pore Size and Volume Distribution in 92% TD Irradiated Pellets from Rod 6 of IFA-431 (error bars = 2σ SD)

37

TABLE 5. Porosity Distribution in Irradiated Pellet 39 from Rod 6 of IFA-431[a]

Porosity Volume, %	Periphery	Midradius	Axial
By Density Measurement[b]	10.4	7.1	6.6
By Pore Measurement	6.4 ±1.6	6.0 ±0.5	6.3 ±0.7
Pores <1 μm	0.7	0.6	0.3
Pores >1 μm	5.7 ±1.6	5.4 ±0.5	6.0 ±0.7
Pores >10 μm	2.5 ±1.6	2.5 ±0.5	2.1 ±0.6

Pore Diameter, μm			
Median, all	5.4	5.4	7.0
Median, <1 μm	0.9	0.9	0.9
Median, >1 μm	7.0	7.0	7.0
Median, >10 μm	58	27	45
Maximum	111	66	85

Pore Population, no./cm^3			
All Pores >0.070 μm	1.13 ±0.06 x 10^{12}	0.23 ±0.11 x 10^{12}	0.08 ±0.15 x 10^{12}
Pores >1 μm	0.79 ±0.09 x 10^{10}	0.78 ±0.14 x 10^{10}	0.40 ±0.06 x 10^{10}
Pores >10 μm	4.0 ±4.4 x 10^6	8.7 ±5.1 x 10^6	2.9 ±6.3 x 10^6

(a) Confidence intervals = 1σ SD, based on image analysis calculations only.
(b) Calculated from densities measured at Harwell on small core samples removed from the respective locations on the polished pellet after completion of microscopy (Reference 11).

The behavior of pellets 13 and 39 is similar and is supported qualitatively by the photomicrographs obtained at Harwell (Figures 17 and 18). Harwell immersion density data obtained from core samples cannot be supported. For example, the midradius microstructure of pellet 13 obviously contains more than 0.4% porosity (see Figure 18).

Figure 23 summarizes all the previous data by showing a comparison of the total pore volume and the pore volume distribution in the as-sintered and irradiated pellets. The general relationships shown are consistent with the

38

TABLE 6. Porosity Distribution in Irradiated Pellet 13 from
Rod 6 of IFA-431[a]

Porosity Volume, %	Periphery	Midradius	Axial
By Density Measurement[b]	7.6	0.4	6.3
By Pore Measurement	4.1 ±0.5	3.9 ±0.6	4.4 ±0.5
Pores <1 μm	0.5	0.2	0.8
Pores >1 μm	3.6 ±0.5	3.7 ±0.6	3.6 ±0.5
Pores >10 μm	2.0 ±0.5	1.9 ±0.6	1.6 ±0.5

Pore Diameter, μm			
Median, all	5.0	7.1	4.2
Median, <1 μm	0.9	0.9	0.9
Median, >1 μm	20	12	7.1
Median, >10 μm	45	45	35
Maximum	66	86	51

Pore Population, no./cm^3			
All Pores >0.070 μm	$0.12 \pm 0.05 \times 10^{12}$	$0.25 \pm 0.14 \times 10^{12}$	$0.20 \pm 1.4 \times 10^{12}$
Pores >1 μm	$0.33 \pm 0.02 \times 10^{10}$	$0.18 \pm 0.01 \times 10^{10}$	$0.30 \pm 0.02 \times 10^{10}$
Pores >10 μm	$0.86 \pm 5.6 \times 10^6$	$2.2 \pm 5.4 \times 10^6$	$1.8 \pm 5.9 \times 10^6$

(a) Confidence intervals = 1σ SD, based on image analysis calculations only.
(b) Calculated from densities measured at Harwell on small core samples removed
    from the respective locations on the polished pellet after completion of
    microscopy (Reference 11).

conclusions that densification clearly occurred in pellets 13 and 39. While
the difference between the precharacterization pellets observed at PNL and the
archive pellet observed at Harwell is disturbing, the probable explanation
given earlier (that the small pores present were not satisfactorily observed
at Harwell) still appears applicable. In any case, the differences observed
in the irradiated pellets (whether compared to PNL or Harwell precharacteriza-
tion information) are still reasonable and consistent within the data set.

39
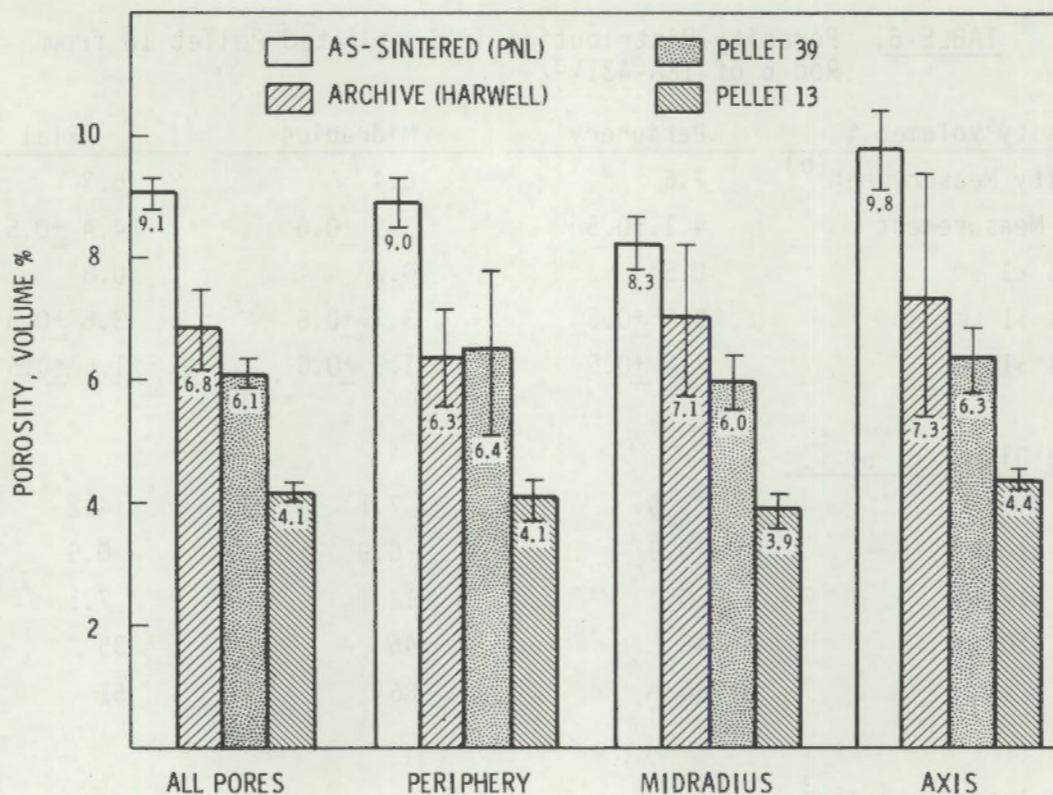
FIGURE 23. Comparison of Total Pore Volume and Pore Volume Distribution in 92% TD As-Sintered and Irradiated Pellets

The pore population relationship between and within preirradiation and irradiated pellets is illustrated in Figures 24 and 25. Previously discussed data from Tables 3 and 4 applies.

To obtain grain size information, the pellets were subsequently etched specifically for grain size definition; measurements were made by the linear intercept technique used in previous work. Table 7 summarizes the measurements from photomicrographs of the type illustrated in Figures 19 and 20. The resulting grain size in the irradiated pellets is only slightly increased or unchanged from preirradiation dimensions. The grain size increase certainly did not approach that achieved in the resintering tests applied to the similar fuel type. From that observation it can be concluded that the temperature within pellets 13 and 39 did not approach the 1873 or 1973K applied in the resintering tests.
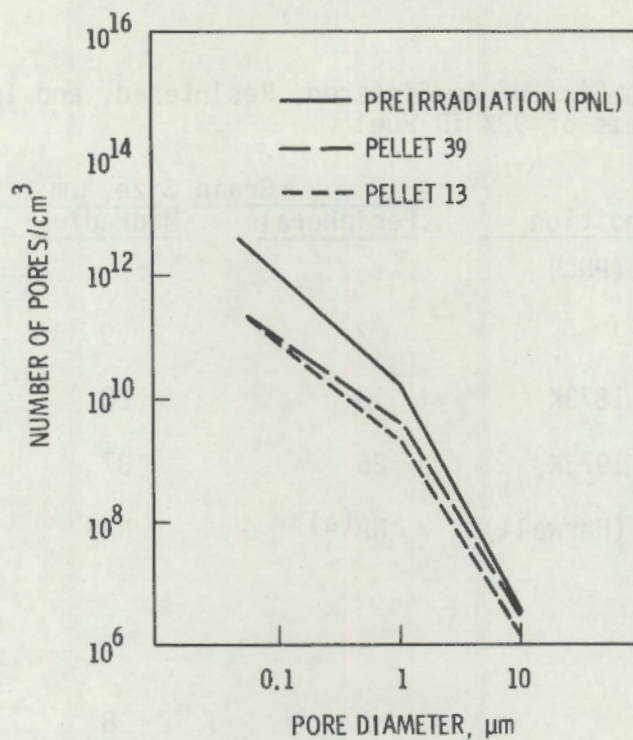
FIGURE 24. Change in Cumulative Pore Population of 92% TD Pellets During Irradiation
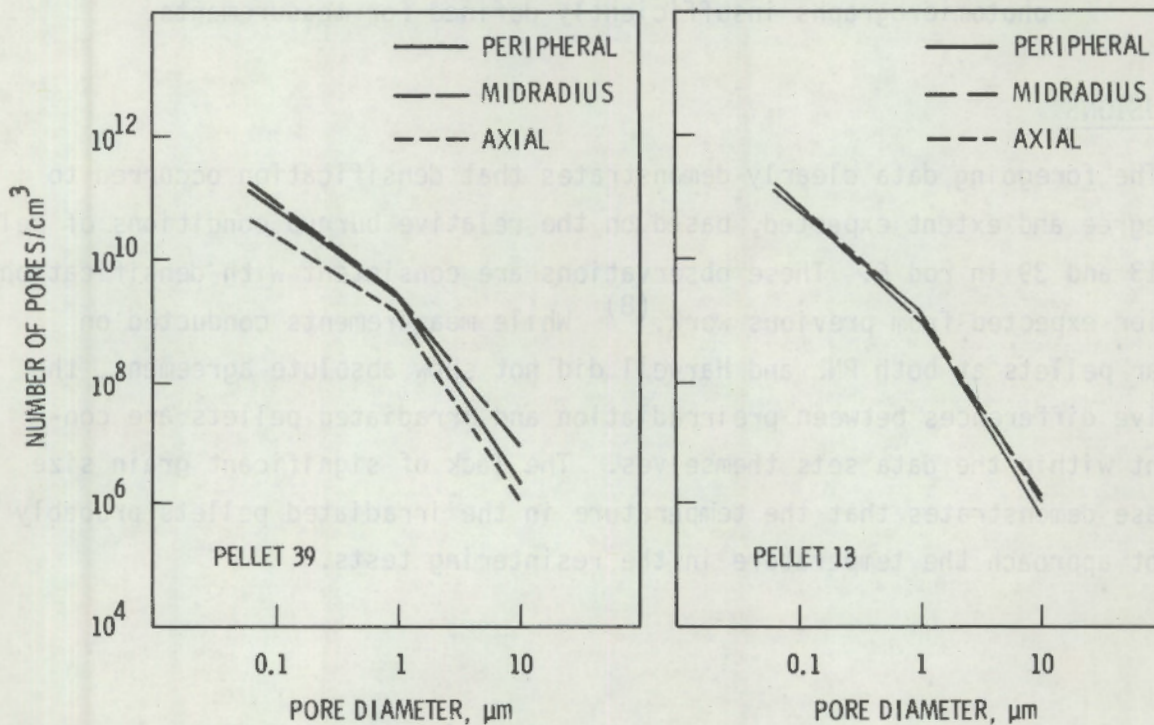
FIGURE 25. Radial Distribution of Pore Population of 92% TD Irradiated Pellets

41

TABLE 7. Grain Size of As-Sintered, Resintered, and Irradiated
Pellets of 92% TD Fuel

Specimen Condition	Grain Size, μm		
	Peripheral	Midradius	Axial
Preirradiated (PNL)			
As-Sintered	2	9	7
Resintered, 1873K	13	20	15
Resintered, 1973K	26	37	53
Preirradiated (Harwell)	NA(a)	NA	NA
Archive			
Irradiated			
Pellet 39	8	8	8
Pellet 13	7	7	8

(a) Not available; grain boundaries on etched specimen
    photomicrographs insufficiently defined for measurements.

CONCLUSIONS

The foregoing data clearly demonstrates that densification occurred to
the degree and extent expected, based on the relative burnup conditions of pel-
lets 13 and 39 in rod 6. These observations are consistent with densification
behavior expected from previous work.[8] While measurements conducted on
similar pellets at both PNL and Harwell did not show absolute agreement, the
relative differences between preirradiation and irradiated pellets are con-
sistent within the data sets themselves. The lack of significant grain size
increase demonstrates that the temperature in the irradiated pellets probably
did not approach the temperature in the resintering tests.

42

COMPUTER CODE COMPARISONS TO THERMAL DATA

Because densification has been observed to affect the thermal and mechanical performance of fuel rods, it is important that computer codes used for design and safety studies be able to model densification effects adequately. It is therefore of interest to compare the data from rod 6 of IFA-431 to fuel rod thermal performance computer code calculations. For this comparison, the following codes used by the NRC were selected: GAPCON-THERMAL-3 (GT3),[14] FRAPCON-1,[15] and FRAPCON-2 (Version 1, Mod 2).[16] Of principal consideration is the comparison of calculated centerline temperatures to those measured in-reactor.

The input for fuel thermal performance codes generally consists of fuel rod dimensions, material properties (including initial fuel density), and operating conditions (power and coolant). When comparing the codes to data, initial dimensions, material properties, and coolant conditions are usually fairly well known. The most difficult problem is supplying the code with an appropriate power history based on the as-measured history.

The as-measured power history for rod 6 of IFA-431 is presented in Figure 26 as a function of time at power (i.e., time at shutdown is not included). The solid line in the figure is the selected power history to be used during the data/code comparison. The centerline temperatures corresponding to the power history are presented in Figure 27. The solid line in this figure is the temperature history to be compared to the code results. The selected power history and corresponding centerline temperatures are listed in Table 8.

Additional input parameters that are needed and common to all three codes of interest are listed in Table 9. Two of the codes--GT3 and FRAPCON-2--allow user input to control the amount of densification calculated during code operation; this input is based on observed densification changes. Two density changes have been observed for the 92% TD unstable fuel used in rod 6.

- During the fuel precharacterization for IFA-431/432,[12] an average final density of 95.3% TD was observed after resintering at 1973K for 24 h.

- PIE showed an average final density of 96.5% TD.

43
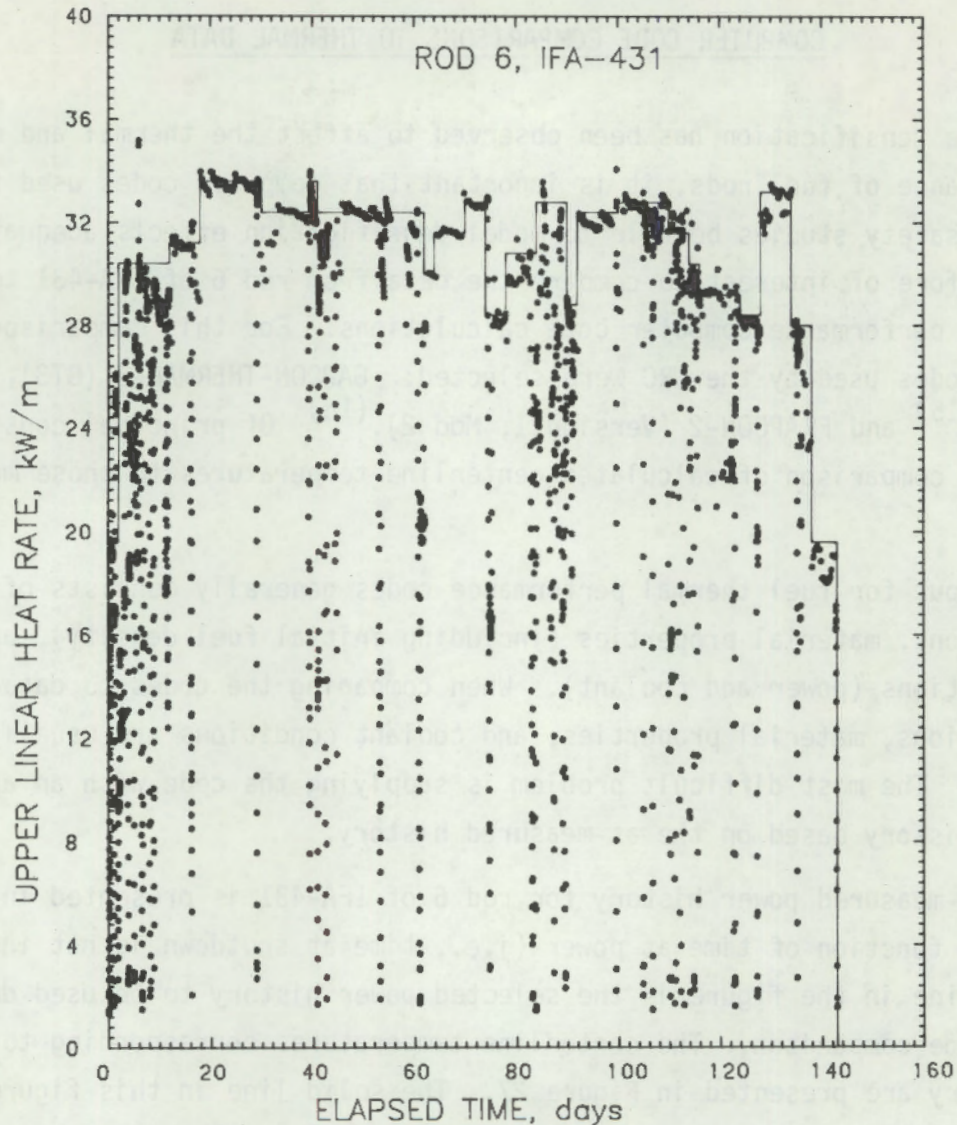
FIGURE 26. Actual Power History and Power History Used for Code Comparison

Densification in GT3 is controlled by inputting the final density, using the time-dependent model of Meyer[10] to apply densification. Three GT3 calculations will be compared to the data: no densification (input variable FRDEN2[a] = 92%), final densification equal to that observed from the thermal resintering tests (FRDEN2 = 95.3%), and final densification equal to that observed from PIE (FRDEN2 = 96.5%).

_____

(a) Input variable FRDEN is used for the initial density and is equal to 92% for these calculations; FRDEN2 specifies the density after densification is complete.

44
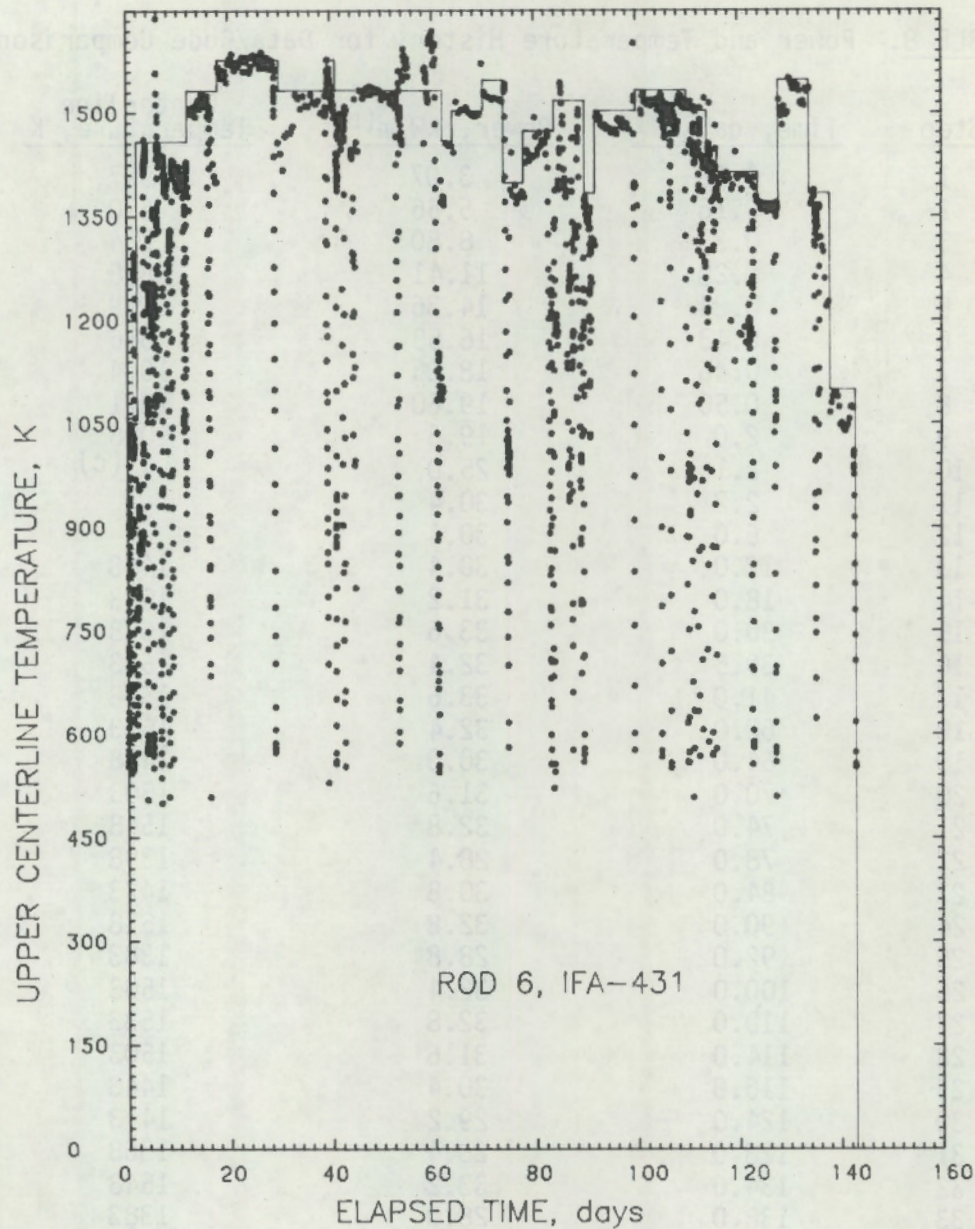
FIGURE 27. Actual Temperature History and Temperature History
Used for Code Comparison

Densification in FRAPCON-2 is calculated by the MATPRO[17] routine FUDENS using either the initial density and sintering temperature or the observed density change during a 1973K 24-h resintering test; the second method is recommended. The observed density of 95.3% TD after resintering at 1973K for 24 h is equivalent to a density increase of 362 kg/m^3 (input variable RSNTR).

45

TABLE 8. Power and Temperature History for Data/Code Comparison

Step	Time, days[a]	Power, kW/m[b]	Centerline Temperature, K
1	0.08	3.07	597
2	0.16	5.66	670
3	0.23	8.80	764
4	0.28	11.41	828
5	0.34	14.36	899
6	0.43	16.58	956
7	0.46	18.05	1004
8	0.50	19.60	1041
9	2.0	19.6	1058
10	2.1	25.0	--[c]
11	2.2	30.4	--
12	6.0	30.4	--
13	12.0	30.4	1458
14	18.0	31.2	1533
15	30.0	33.6	1578
16	39.5	32.4	1533
17	41.0	33.6	1578
18	62.0	32.4	1533
19	64.0	30.0	1458
20	70.0	31.6	1503
21	74.0	32.8	1548
22	78.0	28.4	1398
23	84.0	30.8	1473
24	90.0	32.8	1518
25	92.0	28.8	1383
26	100.0	32.4	1503
27	110.0	32.8	1533
28	114.0	31.6	1503
29	116.0	30.4	1443
30	124.0	29.2	1413
31	128.0	28.4	1368
32	134.0	33.2	1548
33	138.0	28.0	1383
34	143.0	19.6	1098

(a) Time, power, and temperature are for the end of each step.
(b) Steps 1 through 8 are taken from startup data; steps 9 through 34 are taken from Figures 26 and 27.
(c) Steps 10 through 12 are necessary for code operation and were not compared to the data.

46

TABLE 9. Common Input Parameters for Data/Code Comparison

Fuel Dimensions:

cladding outer diameter	12.79 mm
cladding inner diameter	10.91 mm
fuel diameter	10.68 mm
fuel length	571.5 mm
plenum volume	1.64 cm^3

Materials:

initial UO$_2$ density	92% TD
^{235}U enrichment	10%
fill gas	100% He at 0.1 MPa

Operating Conditions:

coolant temperature	513K
coolant pressure	3.4 MPa
axial power profile	see Reference 12
power history	see Table 8

FRAPCON-2 contains three mechanical response packages, which complicates its comparison to the data.[a] Each package has a different effect on calculated temperatures and implements the densification calculated by FUDENS differently. Thus, to implement the densification options and the mechanical package options, three densification assumptions were combined with the PELET and FRACAS-2 mechanical packages: no densification, densification based on the thermal resintering data (RSNTR = 362 kg/m^3), and densification based on the sintering temperature (RSNTR = 0 kg/m^3). The series of calculations that were made are summarized in Table 10.

_____

(a) FRAPCON-2 is a cooperative effort between PNL and the Idaho National Engineering Laboratory (INEL). Each laboratory has developed its own model of fuel rod mechanical response, and the NRC has requested that both models be placed in FRAPCON-2 for evaluation.[18,19] The PELET mechanical package was developed by PNL, and the FRACAS-1 and FRACAS-2 mechanical packages were developed by INEL.

TABLE 10. Computer Runs for Data/Code Comparison

Case	Code	Mechanical Option	Densification Option
1	GT3	none	no densification (FRDEN2 = 92% TD)
2	GT3	none	ex-reactor densification (FRDEN2 = 95.3% TD)
3	GT3	none	in-reactor densification (FRDEN2 = 96.5% TD)
4	FRAPCON-1	none	none (RSNTR = 0)
5	FRAPCON-2	PELET[a]	no densification (RSNTR = 0.01 kg/m^3)
6	FRAPCON-2	PELET	default densification (RSNTR = 0.0 kg/m^3)
7	FRAPCON-2	PELET	ex-reactor densification (RSNTR = 362.0 kg/m^3)
8	FRAPCON-2	FRACAS-2[b]	no densification (RSNTR = 0.01 kg/m^3)
9	FRAPCON-2	FRACAS-2	default densification (RSNTR = 0.0 kg/m^3)
10	FRAPCON-2	FRACAS-2	ex-reactor densification (RSNTR = 362.0 kg/m^3)

(a) PELET developed by PNL.
(b) FRACAS-2 developed by INEL.

Results from the 10 cases that were run are summarized in Table 11. The data is from the upper thermocouple (high-power region) of rod 6 of IFA-431, and the code calculations correspond to that thermocouple location. In general, the following results were obtained:

- GT3 without densification (case 1) undercalculated temperatures while GT3 with densification (cases 2 and 3) overcalculated temperatures.

- FRAPCON-1 (case 4) overcalculated temperatures.

- FRAPCON-2/PELET without densification (case 5) overcalculated temperatures and undercalculated temperatures with densification (cases 6 and 7).

- FRAPCON-2/FRACAS-2 overcalculated temperatures (cases 8, 9, and 10).

The comparisons are more easily seen in Table 12 where the difference between the code calculations and data is presented. Minimum differences occurred for the FRAPCON-2/FRACAS-2 run without densification (case 8) and the GT3 run using ex-reactor thermal resintering densification (case 2).

48

TABLE 11. Results of Data/Code Comparison

Centerline Temperature, K

Step	Data[a]	GT3			FRAPCON-1	FRAPCON-2/PELET			FRAPCON-2/FRACAS-2		
		Case 1[b]	Case 2	Case 3	Case 4	Case 5	Case 6	Case 7	Case 8	Case 9	Case 10
1	597	604	604	604	612	603	603	603	592	592	592
2	670	680	680	680	704	681	681	681	663	663	663
3	764	776	776	776	821	781	781	781	754	754	754
4	828	858	858	858	924	861	861	861	833	833	833
5	899	952	952	952	1044	955	955	955	925	925	925
6	956	1022	1022	1022	1137	1026	1026	1026	997	997	997
7	1004	1069	1069	1074	1199	1073	1073	1073	1046	1046	1046
8	1041	1120	1120	1132	1267	1122	1122	1122	1098	1098	1098
9	1058	1107	1130	1194	1266	1122	1077	1088	1098	1114	1109
10	--[c]	1280	1312	1394	1474	1290	1216	1236	1280	1311	1300
11	--	1451	1493	1591	1670	1456	1362	1389	1465	1507	1492
12	--	1406	1512	1629	1671	1460	1308	1332	1465	1544	1523
13	1458	1365	1512	1642	1673	1459	1270	1289	1465	1576	1552
14	1533	1368	1537	1670	1703	1482	1272	1289	1492	1586	1604
15	1578	1399	1626	1767	1837	1554	1322	1331	1573	1662	1642
16	1533	1357	1592	1723	1817	1523	1288	1296	1534	1620	1602
17	1578	1386	1636	1772	1855	1560	1321	1329	1576	1667	1647
18	1533	1348	1604	1741	1849	1530	1290	1298	1538	1625	1606
19	1485	1287	1522	1655	1764	1465	1229	1236	1460	1535	1518
20	1503	1328	1576	1715	1828	1517	1274	1283	1517	1599	1581
21	1548	1356	1618	1779	1866	1562	1312	1320	1561	1649	1630
22	1398	1245	1468	1621	1711	1443	1200	1208	1414	1483	1468
23	1473	1308	1551	1713	1805	1521	1268	1277	1501	1577	1561
24	1518	1353	1623	1874	1875	1594	1325	1339	1574	1660	1643
25	1383	1256	1487	1732	1734	1491	1230	1238	1441	1509	1495
26	1503	1343	1611	1879	1870	1608	1328	1345	1570	1654	1637
27	1533	1334	1631	1973	1886	1643	1344	1369	1591	1674	1655
28	1503	1320	1591	1935	1847	1626	1322	1347	1555	1631	1614
29	1443	1291	1551	1894	1806	1605	1299	1324	1519	1590	1573
30	1413	1261	1510	1860	1766	1585	1275	1300	1484	1549	1535
31	1368	1243	1484	1834	1738	1576	1263	1288	1462	1524	1511
32	1548	1382	1662	2260	1908	1748	1413	1440	1608	1716	1696
33	1383	1197	1489	2128	1720	1607	1277	1303	1431	1509	1496
34	1098	1020	1200	1840	1407	1331	1040	1062	1135	1184	1177

(a) Upper thermocouple.
(b) See Table 10 for definition of cases.
(c) Steps 10, 11, and 12 were needed for code operation and were not compared to the data.

49

TABLE 12. Comparison of Data and Code Results

Difference Between Code Calculation and Data,[a] K

Step	GT3 Case 1	GT3 Case 2	GT3 Case 3	FRAPCON-1 Case 4	FRAPCON-2/PELET Case 5	FRAPCON-2/PELET Case 6	FRAPCON-2/PELET Case 7	FRAPCON-2/FRACAS-2 Case 8	FRAPCON-2/FRACAS-2 Case 9	FRAPCON-2/FRACAS-2 Case 10
1	7	7	7	15	6	6	6	-5	-5	-5
2	10	10	10	34	11	11	11	-7	-7	-7
3	12	12	12	57	15	15	15	-10	-10	10
4	30	30	30	96	33	33	33	5	5	5
5	53	53	53	145	56	56	56	26	26	26
6	66	66	66	181	70	70	70	41	41	41
7	65	65	70	195	69	69	69	42	42	42
8	79	79	91	226	81	81	81	57	57	57
9	49	72	136	208	64	19	30	40	56	51
10	--[b]	--	--	--	--	--	--	--	--	--
11	--	--	--	--	--	--	--	--	--	--
12	--	--	--	--	--	--	--	--	--	--
13	-93	54	184	215	1	-188	-169	7	118	94
14	-170	4	137	170	-51	-261	-244	-41	53	71
15	-179	48	189	259	-24	-256	-247	-5	84	64
16	-176	59	190	284	-10	-245	-237	1	87	69
17	-192	58	194	277	-18	-257	-249	-2	89	69
18	-185	71	208	316	-3	-243	-235	5	92	73
19	-171	37	170	279	7	-229	-222	2	77	60
20	-175	73	212	325	14	-229	-220	14	96	78
21	-192	70	231	318	14	-236	-228	13	101	82
22	-153	70	223	313	45	-198	-190	16	85	70
23	-165	78	240	332	48	-205	-196	28	104	88
24	-165	105	356	357	76	-193	-179	56	142	125
25	-127	104	349	351	108	-153	-145	58	126	112
26	-160	108	376	367	105	-175	-158	67	151	134
27	-199	98	440	353	110	-189	-164	58	141	122
28	-183	88	432	344	123	-181	-156	52	128	111
29	-152	108	451	363	162	-144	-119	76	147	130
30	-152	97	447	353	172	-138	-113	71	136	122
31	-125	116	466	370	208	-105	-80	94	156	143
32	-166	114	712	360	200	-135	-108	60	168	148
33	-186	106	745	337	224	-106	-80	48	126	113
34	-78	102	742	309	233	-58	-36	37	86	79

(a) A positive difference means the code calculation was greater than the data.
(b) Steps 10, 11 and 12 were needed for code operation and were not compared to the data.

50

When densification is used in conjunction with FRAPCON-2/PELET, the calculated temperatures are less than when no densification is assumed due to the fuel model used in PELET[a] (see Table 12). Densification is applied by reducing the cold fuel diameter and thus increasing the amount of voidage, which increases the roughness and widths of the fuel cracks and the fuel-cladding gap. However, an increase in the interaction between fuel fragments apparently accompanies the increased roughness, which increases the effective fuel thermal conductivity and reduces fuel temperatures.

When comparing data and code calculations, it is possible to define a band around the data within which a code calculation can be accepted. Two possible ways to define this acceptance band are:

- the uncertainty in the temperature measurement

- the uncertainty in the expected operating temperature given the uncertainty in fuel rod dimensions, material properties, and operating conditions.

The first definition results in a narrow band and requires that the code calculate the behavior of a specific rod that may or may not be typical of that design. The second definition results in a wider acceptance band that accounts for the expected behavior differences in nominally identical rods. Use of this second acceptance band allows the code to be compared to the expected general response of a rod design based on the actual specific response of that rod design.

Table 13 details the widths of the two acceptance bands. For the first band, the temperature measurement uncertainty is reported to be $\pm 3\%$ at a confidence level of 3σ (99.7% confidence level),[20] which corresponds to approximately ± 35 to ± 40K during the steady-state portion of the irradiation.

The second acceptance band was determined by applying linear propagation of errors to the calculation of fuel temperature.[21,22] By requiring that

_____

(a) A complete discussion of the PELET mechanical package may be found in Reference 16.

51

TABLE 13. Acceptance Bands for Data/Code Comparison

Step	Centerline Temperature, K	Temperature Measurement Uncertainty, K[a]	Calculated Operational Uncertainty[b]
1	597	10	33
2	670	12	35
3	764	15	50
4	828	17	57
5	899	19	64
6	956	20	70
7	1004	22	75
8	1041	23	79
9	1058	24	82
10	--[c]	--	--
11	--	--	--
12	--	--	--
13	1458	36	137
14	1533	38	151
15	1578	39	154
16	1533	38	147
17	1578	39	154
18	1533	38	147
19	1485	36	139
20	1503	37	144
21	1548	38	149
22	1398	34	131
23	1473	36	140
24	1518	37	143
25	1383	33	127
26	1503	37	141
27	1533	38	146
28	1503	37	144
29	1443	35	135
30	1413	34	132
31	1368	33	124
32	1548	38	148
33	1383	33	129
34	1098	25	92

(a) Temperatures were measured in $^{\circ}C$ and uncertainty is based on as-measured temperatures.
(b) Calculation was performed in $^{\circ}C$; power uncertainty = 5.6% (Reference 20); and 3 confidence level.
(c) Steps 10, 11, and 12 were needed for code operation and were not compared to the data.

the calculated centerline temperature match the data, the resulting uncertainty calculation can be interpreted as the expected range of temperature response given the dimensional and operating uncertainties. A code calculation that falls within this band ($\sim\pm140$K) is assumed to be reasonable.

By comparing Tables 12 and 13, it is possible to make the following statements about the thermal performance of the codes relative to the data.

- GT3 - If run without allowing densification, the calculated temperatures lie within the acceptance band during the rise to power. However, calculated temperatures are below the band throughout the steady-state irradiation. If run with a final density of 95.3% TD (thermal resintering result), the calculations lie within the acceptance band until the last step. Inputting a final density of 96.5% TD (from PIE) results in a strong overcalculation of temperature.

- FRAPCON-1 - Temperatures are greatly overcalculated using the default densification.

- FRAPCON-2/PELET - If run without densification, the calculated temperatures lie within the acceptance band until late in the power history, at which point temperatures are overcalculated. If run with either densification option, calculated temperatures are within the acceptance band during the rise to power. During steady-state irradiation, temperatures are undercalculated until late in the power history.[a]

- FRAPCON-2/FRACAS-2 - Except for scattered points late in the power history, calculated temperatures (with and without densification) lie within the acceptance band.

_____

(a) Following the completion of this work and prior to publication, the anomalous result of densification that had caused a decrease in the calculated temperatures was traced to an error in the publicly available version of FRAPCON-2 (Version 1, Mod 2). With the error corrected, FRAPCON-2/PELET temperatures (with RSNTR = 362 kg/m^3) increased to values greater than the data but within the acceptance band until power history step 25. The effect of porosity changes within the PELET/RADIAL model is under review.

REFERENCES

1. U.S. AEC Regulatory Staff. November 1972. Technical Report on Densification of Light Water Reactor Fuels. Washington, D.C.

2. Ditmore, D. C., and R. B. Elkins. December 1972. Densification Considerations in Boiling Water Reactor Fuel Design and Performance. NEDM-10735, General Electric Co., San Jose, California.

3. U.S. AEC Regulatory Staff. September 1973. Technical Report on Densification of Exxon Nuclear BWR Fuels. Washington, D.C.

4. Buescher, B. J., and J. W. Pegram. July 1977. Babcock & Wilcox Model for Predicting In-Reactor Densification. BAW-10083A, Rev. 1, Babcock & Wilcox, Lynchburg, Virginia.

5. Stehle, H., and H. Assman. 1974. "The Dependence of In-Reactor UO_2 Densification on Temperature and Microstructure." J. of Nuclear Materials 52:303-308.

6. Storhok, V. W. December 1974. Final Report on a Study of In-Reactor Densification of UO_2 Fuel in the MH-1A Reactor. Battelle-Columbus Laboratories, Columbus, Ohio.

7. "A Summary of CE Work on In-Pile Densification of Uranium Dioxide." Paper presented at the Government/Industry Working Meeting on UO_2 and ThO_2 Fuel Performance Technology, January 29-30, 1976, ERDA, Germantown, Maryland.

8. Freshley, M. D., et al. November 1976. "Irradiation-Induced Densification of UO_2 Pellet Fuel." J. of Nuclear Materials 62:138-166.

9. Lindman, N. 1977. "On the Rate of In-Reactor UO_2 Densification." J. of Nuclear Materials 71:73-77.

10. Meyer, R. O. July 1976. The Analysis of Fuel Densification. NUREG-0085, U.S. Nuclear Regulatory Commission, Washington, D.C.

11. Neally, C., et al. October 1979. Post-Irradiation Data Analysis for NRC/PNL Halden Assembly IFA-431. NUREG/CR-0797, PNL-2975, Pacific Northwest Laboratory, Richland, Washington.

12. Hann, C. R., et al. November 1977. Test Design, Precharacterization, and Fuel Assembly Fabrication for Instrumented Fuel Assemblies IFA-431 and IFA-432. NUREG/CR-0332, BNWL-1988, Pacific Northwest Laboratory, Richland, Washington.

13. Lanning, D. D., B. O. Barnes, and R. E. Williford. January 1979. Manifestations of Nonlinearity in Fuel Center Thermocouple Steady-State and Transient Data: Implications for Data Analysis. NUREG/CR-0220, PNL-2692, Pacific Northwest Laboratory, Richland, Washington.

14. Lanning, D. D., et al. January 1978. GAPCON-THERMAL-3 Code Description. PNL-2434, Pacific Northwest Laboratory, Richland, Washington.

15. Berna, G. A., et al. June 1980. FRAPCON-1: A Computer Code for the Steady State Analysis of Oxide Fuel Rods. NUREG/CR-1463, EGG-2039, Idaho National Engineering Laboratory, Idaho Falls, Idaho.

16. Berna, G. A., et al. December 1980. FRAPCON-2: A Computer Code for the Calculation of Steady State Thermal-Mechanical Behavior of Oxide Fuel Rods. NUREG/CR-1845, U.S. Nuclear Regulatory Commission, Washington, D.C.

17. Reymann, G. A., ed. February 1978. MATPRO-Version 10: A Handbook of Materials Properties for Use in the Analysis of Light Water Reactor Fuel Rod Behavior. TREE-NUREG-1180, Idaho National Engineering Laboratory, Idaho Falls, Idaho.

18. Berna, G. A., D. D. Lanning, and W. N. Rausch. June 1981. FRAPCON-2 Developmental Assessment. NUREG/CR-1949, Pacific Northwest Laboratory, Richland, Washington.

19. Laats, E. T., et al. July 1981. Independent Assessment of the Steady-State Fuel Rod Analysis Code FRAPCON-2. EGG-CAAP-5335, EG&G Idaho, Inc., Idaho Falls, Idaho.

20. Hann, C. R., et al. February 1977. A Method for Determining the Uncertainty of Gap Conductance Deduced from Measured Centerline Temperatures. BNWL-2091, Pacific Northwest Laboratory, Richland, Washington.

21. Cunningham, M. E., et al. May 1978. Stored Energy Calculation: The State of the Art. NUREG/CR-0320, PNL-2581, Pacific Northwest Laboratory, Richland, Washington.

22. Cunningham, M. E., et al. September 1980. Application of Linear Propagation of Errors to Fuel Rod Temperature and Stored Energy Calculations. NUREG/CR-1753, PNL-3539, Pacific Northwest Laboratory, Richland, Washington.

DISTRIBUTION

No. of
Copies

OFFSITE

A. A. Churm
DOE Patent Division
9300 S. Cass Avenue
Argonne, IL 60439

400 U.S. Nuclear Regulatory
Commission
Division of Technical
Information and Document
Control
7920 Norfolk Avenue
Bethesda, MD 20014

2 DOE Technical Information Center

4 G. P. Marino, Chief
Fuel Behavior Research Branch
Division of Reactor Safety
Research
U.S. Nuclear Regulatory
Commission
Washington, DC 20555

H. H. Scott
Division of Reactor Safety
Research
U.S. Nuclear Regulatory
Commission
Washington, DC 20555

No. of
Copies

R. Van Houton
Fuel Behavior Research Branch
Division of Reactor Safety
Research
U.S. Nuclear Regulatory
Commission
Washington, DC 20555

ONSITE

50 Pacific Northwest Laboratory

W. J. Bailey
J. O. Barner
E. R. Bradley
M. E. Cunningham (25)
J. L. Daniel
S. K. Edler
M. D. Freshley
R. L. Goodman
R. J. Guenther
C. R. Hann
D. D. Lanning
R. K. Marshall
C. L. Mohr
C. Nealley
F. E. Panisko
W. N. Rausch
R. E. Schreiber
R. E. Williford
C. L. Wilson
Publishing Coordination (2)
Technical Information YO(5)

NRC FORM 335 (7 77)	U.S. NUCLEAR REGULATORY COMMISSION **BIBLIOGRAPHIC DATA SHEET**	1. REPORT NUMBER (Assigned by DDC) NUREG/CR-2042 PNL-3782

4. TITLE AND SUBTITLE (Add Volume No., if appropriate) Observation of Porosity Reduction in a Densification-Prone Test Fuel Rod: Data and Analysis	2. (Leave blank)
	3. RECIPIENT'S ACCESSION NO.

7. AUTHOR(S) M.E. Cunningham, J.L. Daniel, D.D. Lanning	5. DATE REPORT COMPLETED
	MONTH September	YEAR 1981

9. PERFORMING ORGANIZATION NAME AND MAILING ADDRESS (Include Zip Code) Pacific Northwest Laboratory Richland, WA 99352	DATE REPORT ISSUED
	MONTH October	YEAR 1981
	6. (Leave blank)
	8. (Leave blank)

12. SPONSORING ORGANIZATION NAME AND MAILING ADDRESS (Include Zip Code) Division of Accident Evaluation Office of Nuclear Regulatory Research U.S. Nuclear Regulatory Commission Washington, DC 20555	10. PROJECT/TASK/WORK UNIT NO
	11. CONTRACT NO. FIN B2043

13. TYPE OF REPORT	PERIOD COVERED (Inclusive dates)

15. SUPPLEMENTARY NOTES	14. (Leave blank)

16. ABSTRACT (200 words or less)

Instrumented fuel assembly (IFA)-431 was irradiated in the Halden Boiling Water Reactor (HBWR) for the purpose of extending the steady-state data base. Rod 6 of this assembly began irradiation with UO_2 fuel of 92% theoretical density (TD) that was unstable with respect to in-reactor densification. Thermal resintering tests resulted in a final density of 95.3% TD while post-irradiation examination (PIE) indicated a final density of 96.5% TD. Observed microstructural changes were consistent with published densification studies; there was a marked depletion of submicrometer diameter pores and total pore volume. However, grain size increased only slightly, indicating that internal pellet temperatures did not reach the 1875K applied in resintering tests.

17. KEY WORDS AND DOCUMENT ANALYSIS	17a DESCRIPTORS

17b. IDENTIFIERS/OPEN-ENDED TERMS

18. AVAILABILITY STATEMENT Unlimited	19. SECURITY CLASS (This report) Unclassified	21. NO. OF PAGES
	20 SECURITY CLASS (This page) Unclassified	22 PRICE S

NRC FORM 335 (7 77)